

ORIGIN OF TIDAL DISSIPATION IN JUPITER: II. THE VALUE OF Q

Yanqin Wu

Department of Astronomy and Astrophysics, 60 St. George Street, University of Toronto, Toronto, ON M 5S 3H 8, Canada

Draft version May 23, 2019

ABSTRACT

Having studied the structure and properties of inertial modes in a neutrally buoyant, uniformly rotating sphere (Wu 2004), we examine here their effect on tidal dissipation in Jupiter. The rate of tidal dissipation caused by resonantly excited inertial modes depends on the following three parameters: how well coupled inertial modes are to the tidal potential, how strongly dissipated inertial modes are by the turbulent viscosity, and how densely distributed the inertial modes are in frequency. Our analytical and numerical study based on realistic Jupiter models lead us to conclude that, tidal dissipation by inertial modes is three to five orders of magnitude stronger than that caused by the equilibrium tide. The uncertainty in this result mostly arises from uncertainty in the tidal coupling, which depends on the density structure inside Jupiter. In the best-case scenario we have studied, where hydrogen undergoes a first-order molecular/metallic phase transition, the rate of tidal dissipation corresponds to a tidal quality factor $Q \approx 10^7$, approaching the empirically inferred Q value for Jupiter.

We find that as a function of tidal frequency, the tidal Q value exhibits large fluctuations, but its nominal value is determined by inertial modes that satisfy $\omega \approx \omega_c$, where ω_c is the typical frequency of $m=2$ resonance and the turbulent damping rate. These are intermediate order inertial modes with wavenumbers $n \approx 60$ and they can be excited to surface displacement amplitudes of order 10^3 cm. Dissipation of inertial modes occur very close to the surface in a narrow latitudinal zone (the ‘singularity belt’). We therefore expect the tidal luminosity to escape easily from the planet.

We discuss effects of the solid core, radiative atmosphere and prescription for turbulent viscosity on our conclusions. We also compare our results with those from a competing work by (Ogilvie & Lin 2004). We hope to apply the inertial mode theory to extra-solar jupiters, solar-type binaries and other objects where the mechanism for tidal dissipation is not well understood.

Subject headings: hydrodynamics | waves | planets and satellites: individual (Jupiter) | stars: oscillations | stars: rotation | turbulence

1. introduction

1.1. the Puzzle

We tackle the classical problem of tidal dissipation in Jupiter. In the following, we briefly review the problem, both for Jupiter and close-in extra-solar planets. For a contemporary and expansive overview of this issue, including a detailed discussion of previous work, we refer the readers to Ogilvie & Lin (2004, hereafter OL).

As Jupiter spins faster than the orbital motion of its nearest satellite (Io), Io raises a time-dependent tide on Jupiter. The dissipation of this tide in Jupiter transfers its angular momentum to Io and spins down Jupiter. We adopt the convention of quantifying the inefficiency of the dissipation¹ by a dimensionless quality factor Q , which is the ratio between the energy in the (equilibrium) tide and the energy dissipated per period

$$Q = \frac{2E_0}{\frac{dE}{dt}} = \frac{1}{\tan 2\epsilon} \frac{1}{2}; \quad (1)$$

where ϵ is called the lag angle. In the picture of equilibrium tide, ϵ is the angle between the directions of Io and the tidal bulge. The timescale of tidal synchronization scales linearly with Q .

Based on the current resonant configuration of the Galilean satellites, Jupiter’s Q value has been estimated to be $10^5 < Q < 10^6$ with the actual value likely closer to the lower limit (Goldreich & Soter 1966; Peale & Greenberg 1980). The interior of Jupiter is comprised of (at most) a small heavy-element core, a metallic hydrogen region and a molecular hydrogen envelope (see, e.g. Guillot et al. 2004), with convection being the dominant heat transfer mechanism outside the core. The most reliable theoretical estimate of the Q value { based on turbulent viscosity acting on the equilibrium tide { puts $Q \approx 10^3$ (Goldreich & Nicholson 1977), well above the inferred value. The physical origin for this low Q value (and thus high than expected dissipation) has remained elusive for a few decades, with suggestions ranging from a substantial inner core (Demott 1979), to helium hysteresis around the depth of hydrogen metallic phase transition (Stevenson 1983), to a postulated stratification in the interior that harbors rotationally-modified gravity-modes (Ioannou & Lindzen 1993). Each proposal promises interesting implication for the physics of dense matter or for the structure of Jupiter. Where does the truth lie? Intriguingly, Saturn has a similar inferred Q value as Jupiter (Goldreich & Soter 1966).

¹ This assumes Q is independent of the orbital phase. Hut (1981) and others have adopted instead a constant lag time $\tau = \tau_0(1 - f)$, where τ_0 and f are the rotational and instantaneous orbital angular velocity, respectively, and f is the free anomaly. These two approaches are comparable if Q is frequency independent and if the eccentricity is not too large.

The discovery of close-in extra-solar jupiters has rejuvenated our interest in this problem and provided new insights. While the majority of exo-planets are in eccentric orbits around their host stars, the closest-in ones have low or nearly zero eccentricities. This results from the dissipation of stellar tide inside the planets which converts orbital energy into heat without removing orbital angular momentum. Fig. 1 in Wu (2003) shows that the observed upper envelope of planet eccentricity as a function of its semimajor axis can be explained by a tidal quality factor of $Q \sim 3 \times 10^3$ if these are gaseous planets similar to Jupiter in their ages and sizes.²

The close-in exo-planets and Jupiter may well have different formation history, leading to different core sizes and interior compositions. They certainly evolve in very different thermal environments, resulting in diverging thermal structure in their upper atmosphere. Nevertheless, they share similar Q factors. This prompts us to seek a physical explanation for Q which is based on overt similarities between these planets. The first trait in common which we believe is important is that their interiors are fully convective. The second trait is that they rotate fast. Jupiter spins roughly four times for every Io orbit, while the spin of close-in ($a < 0.1\text{AU}$) planets should have long been (pseudo-)synchronized with their orbital motion. So in both cases, the (dominant) tidal forcing frequencies viewed in the planets' rotating frame are below 2.³ Could these two common traits be responsible for the tidal Q values?

1.2. The Inertial Mode Approach

In a spinning and neutrally buoyant fluid sphere, a new branch of eigen-modes arise: the inertial modes. Their motion is restored not by pressure or buoyancy, but by Coriolis force. In the rotating frame, these modes have frequencies ranging from zero to twice the spin frequency. As noted above, the tidal frequencies also fall in this range. How does the presence of these modes affect tidal dissipation?

We have previously studied inertial modes in non-uniform density spheres (Wu 2004, hereafter Paper I), focusing on properties relevant to tidal dissipation. We found that inertial modes that can potentially couple to the tidal potential are much denser in frequency space compared to gravity-or-pressure modes, allowing for good resonance with the tidal forcing. Inertial modes have unique "singularity belts" near the surface where both mode amplitudes and velocity shear are the largest, leading to strong turbulent dissipation. All these indicate that inertial modes are good candidates to explain the tidal dissipation in planets. In this paper, we explore this possibility for Jupiter.

Because of mathematical difficulties, rotation has been largely ignored in tidal theories (for an exception, see Savonije et al. 1995, as well as their subsequent papers). However, this can not be justified when rotational frequency is comparable or faster than the tidal frequency. Tidal response of the fluid will be strongly influenced by rotation. Our results here show that when rotation is taken into account, even the most rudimentary treatment

gives orders of magnitude stronger tidal dissipation than $Q \sim 10^3$.

In this direction, most noteworthy is a recent independent work by O'L, which appeared while we were writing up our results. In this paper, O'L calculated the effect of inertial modes in planets, based on essentially the same physical picture as we consider here. We discuss their work in the context of our results. For un-initiated readers, we recommend their excellent and helpful review of issues related to tidal dissipation and to inertial modes.

1.3. Organization

Paper I has laid a foundation by studying properties of inertial modes. Here, we first summarize relevant results from that paper, then proceed to discuss two issues of importance: how strongly is an inertial mode coupled to the tidal potential, and how strongly is an inertial mode damped by turbulent viscosity (x2). We present contents of highly technical nature in Appendix D, where we also explain our results using a simple toy model. We then discuss our results on tidal Q (x3) for inertial mode dynamical tide, using equilibrium tide as a comparison to illustrate the advantage of inertial modes. Lastly, we discuss possible uncertainties in our model, and compare our results with previous work (x4). We summarize and discuss other possible applications in x5.

2. inertial-modes { relevant properties

Each inertial mode in a uniform-density sphere can be characterized by three quantum numbers, n_1, n_2 and m . Here, n_1 and n_2 are the number of nodes along the x_1 or x_2 ellipsoidal coordinate lines (Bryan 1889), and m is the usual azimuthal number with the perturbations satisfying the form e^{im} and ϕ being the azimuthal angle. For a graphical presentation of an inertial mode, see Figs. 4 & 5 in Paper I. The introduction of ellipsoidal coordinates allows the partial differential equation governing inertial modes in constant density spheres to be separated into two ordinary differential equations. In Paper I, we further extended this capability to spheres of power-law densities ($\rho/\rho_0 = (r/R)^p$), where R is the planet radius and r the spherical radius, and showed that for spheres of smooth but arbitrary density laws, one could obtain sufficiently accurate (albeit approximate) eigenfunctions using these coordinates.

In Paper I, we also introduced mode wavenumber $2(n_1 + n_2)$ and related it to the dimensionless mode frequency $\omega = \Omega \sin(\theta_1)$, where Ω is the inertial mode frequency viewed in the rotating frame, θ_1 the spin frequency, and $0 < \theta_1 < \pi/2$. Under this convention, $m < 0$ denotes retrograde modes, while $m > 0$ prograde ones.

2.1. Goodness of Resonance

Each eigenmode in a non-rotating star is identified by three quantum numbers n, l, m where n is the number of nodes in the radial direction, and l, m relate to the single spherical harmonic function $P_l^m(\cos\theta)$ that describes the angular dependence of the mode. In contrast, the angular dependence of each inertial mode is composed of a

² One exception is the planet HD 80606b whose abnormally high eccentricity may be acquired relatively recently (Wu & Murray 2003).

³ In this respect, it is interesting to point out that tidally circularizing solar-type binaries have convective envelopes and likely spin fast. Curiously, they exhibit similar Q values as these giant planets Mathieu et al. (2004).

series of these spherical harmonic functions. This has the consequence that while only the $l = 2, m = 2$ branch of non-rotating modes can be driven by a potential forcing of the form P_2^2 (the dominant tidal forcing term), every even-parity inertial mode can potentially be driven. In this sense, the frequency spectrum of inertial modes is dense, and the probability of finding a good frequency match (mode frequency = forcing frequency) is much improved over the non-rotating case.

How far in frequency does the closest inertial mode lie from a given forcing frequency ω_0 ? We limit ourselves to inertial modes with $2(n_1 + n_2) \leq m_{\text{ax}}$. Approximate mode frequency by $\sin(n_1) = \omega_0$. Modes with the same n_2 but different n_1 are spaced in frequency by $\Delta\omega = \omega_{\text{ax}}$. Now allow n_2 to vary between 1 and $m_{\text{ax}}/4$, we find that the best frequency ω_0 -resonance to ω_0 is typically

$$(\omega_0)_{\text{min}} = \frac{\omega_{\text{min}}}{2} \sim \frac{\omega_{\text{ax}}}{m_{\text{ax}} n_2} \sim \frac{4}{m_{\text{ax}}^2} : \quad (2)$$

For comparison, gravity- or pressure-modes in non-rotating bodies can at best have a frequency detuning of $\omega = \omega_0 - \omega_{\text{ax}}$ with n being the radial order for the mode of concern.

2.2. Overlap with Tidal Potential

Io orbits Jupiter in the equatorial plane with a frequency $\omega_{\text{Io}} = 2\pi/1.769 \text{ day}^{-1}$ and at a distance a , while Jupiter spins with a frequency $\omega = 2\pi/0.413 \text{ day}^{-1}$. Viewed in Jupiter's rotating frame, Io rotates retrogradely with frequency $\omega^0 = \omega_{\text{Io}} - \omega$ and exerts a periodic tidal forcing on Jupiter. We ignore Io's orbital eccentricity (0.004) in this problem. So at a point $(r; \theta; \phi)$ inside Jupiter, the potential of the tidal perturbation can be decomposed as

$$\begin{aligned} \phi_{\text{Io}} = & \frac{GM_{\text{Io}}}{a} \frac{r}{a} \sin^2 \theta \cos(2\phi + \omega^0 t) \\ & + \frac{3}{2} \frac{r^2}{a^2} \sin^2 \theta - \frac{1}{3} - \frac{3}{2} \frac{r}{a} \sin^2 \theta \\ & + \cos(2\phi + 2\omega^0 t) + O\left(\frac{r^3}{a^3}\right) : \end{aligned} \quad (3)$$

The first term is necessary for maintaining the Keplerian motion of this point in Jupiter; the second term corresponds to the case when Io is smeared into a ring around Jupiter; the third term is the one of relevance here. It describes the periodic forcing by Io in Jupiter's rotating frame. Keeping only this term and writing

$$\phi_{\text{tide}} = \frac{3GM_{\text{Io}}}{2a^3} \xi^2 \cos(2\phi + 2\omega^0 t); \quad (4)$$

we obtain $\omega_{\text{tide}} = \omega_{\text{tide}}^2 = 2\omega^0 = 2\omega = 0.766$ and $m = 2$. Here, $\xi = r \sin \theta$ is the cylindrical radius.

We investigate here the coupling between inertial modes and the above tidal potential. The forcing is integrated over the planet to yield the overlap integral,

$$\begin{aligned} \int_V d^3r \frac{\partial}{\partial t} \phi_{\text{tide}} r_{\text{tide}} &= \int_V d^3r \phi_{\text{tide}} r_{\text{tide}} \quad (5) \\ &= \int_V d^3r \phi_{\text{tide}}^0 = \int_V d^3r \phi_{\text{tide}} \frac{\omega^2}{1P} : \end{aligned}$$

Here, ϕ^0 and ϕ are the inertial mode displacement and Eulerian density perturbation, respectively, and the eigenfunction ϕ is related to ϕ^0 by $\phi^0 = \omega^2 \phi$ (eq. [9] in Paper I). The overlap integral represents the amount of energy gained by a mode.

2.2.1. Tidal Overlap for the Equilibrium Tide

In the limit where ω_{tide} falls well below the dynamical frequency of the planet, its tidal response, except from the resonant part, will approximately satisfy instantaneous hydrostatic equilibrium and is termed the 'equilibrium tide'. The resonant part, where the tidal frequency has a near-resonant match with one of the free modes in the planet, is called the 'dynamical tide'.⁵

Tidal overlap for the equilibrium tide is the largest among all tidal response. Disregard any time derivative in the fluid equation of motion, take $N^2 = 0$ for the neutrally buoyant interior, and assume any perturbation to be adiabatic, we use equations in 2.1 of Paper I to obtain the following instantaneous response,

$$\phi_{\text{equi}}^0 = \frac{2}{1P} \phi_{\text{tide}} : \quad (6)$$

Let the tidal overlap to be E_0 . It is

$$\int_V d^3r \phi_{\text{tide}}^0 \phi_{\text{equi}}^0 = \frac{24}{5} \frac{GM_{\text{Io}}}{a^3} \int_0^2 \int_0^R \frac{r^6}{1P} dr \quad (7)$$

This is the energy stored in the equilibrium tide and it appears in equation (1). Taking $M_{\text{Io}} = 8.93 \times 10^{25} \text{ g}$, $a = 4.22 \times 10^8 \text{ cm}$, and integrating over a model for Jupiter from Guillot et al. (2004), we find $E_0 = 3 \times 10^{10} \text{ erg}$. In comparison, the current potential energy of Io is $3 \times 10^{28} \text{ erg}$. So, over the history of the solar system, Jupiter could have pushed Io outward for a negligible 10^{-7} of its current orbit if the tidal quality factor were as large as $Q = 10^3$.

As a side note, the spatial dependence of the tidal potential, as well as that of the equilibrium tide, can be expressed in the following form which resembles the spatial dependence of an inertial mode in a uniform-density sphere: $\phi_{\text{tide}} / \xi^2 / P_2^2(x_1)P_2^2(x_2)$, here x_1 and x_2 are the aforementioned ellipsoidal coordinates. In comparison, the lowest-order inertial mode ($n_1 = n_2 = 0$, also called a R-mode) has the form $\phi = P_3^2(x_1)P_3^2(x_2)$.

2.2.2. Tidal Overlap for Inertial Modes

Consider first the tidal coupling for a gravity mode in a solar-type star. The overlap with the tidal potential suffers cancellation as neighboring nodal patches contribute to the coupling with opposite phases (ϕ^0 takes opposite signs). The WKBJ region is therefore largely irrelevant and the nodal overlap mostly arises from the upper evanescent region of the mode, which contains the convection zone.

The situation is different for an inertial mode. Such a mode propagates over much of the interior of a planet. Its upper evanescent region is comparable in size to any other nodal region. So the overall tidal overlap is the small residue after the cancellation between various nodes. This

⁴ Unless $\omega_0 = 0$ or $\omega_0 = 1$, we have $n_1 \neq n_2$.

⁵ In essence, the 'equilibrium tide' is equivalent to the sum of all 'dynamical tide' response at a ω_0 -resonance frequency.

property makes it difficult to obtain reliable tidal overlap. In fact, obtaining results in this section has been the most difficult part of this project. Much attention is paid to ensure the accuracy of numerical integrations, and to analytically understand the numerical results.

We delegate most of the technical discussions to the appendices. In appendix xB, we evaluate tidal overlap for inertial modes in a uniform-density model. In appendix xC, we discuss results obtained for models of a single power-law index (γ). Lastly, in appendix xD, we present results for models with more realistic density profiles, including actual Jupiter models. We substantiate our numerical results by studying a simple toy-model where analytical results are available. Here, we list relevant conclusions.

We find that the severity of cancellation rises with increasing mode order. We quantify this severity by the following dimensionless number,

$$C_n = \frac{\int_0^R \frac{1}{\text{tide}} \frac{r^{2n-2}}{r^{2n-2}} dr}{\int_0^R \frac{1}{\text{tide}} \frac{r^{2n-2}}{r^{2n-2}} dr} : \quad (8)$$

While $C_n = 1$ for the equilibrium tide, C_n decreases with rising n (or with rising n where $n = n_1 + n_2$) with a slope that depends on the model. Specifically, integration of the top integral over the spherical surface always gives rise to a cancellation of order n^{-1} , while integration over the radius suffers a cancellation whose magnitude depends on factors including polytropic index of the model and interior inhomogeneities (e.g., density jumps associated with first-order phase transitions, transition of the equation of state).

In a uniform-density sphere, tidal overlap for all modes is zero because the material is incompressible. When we adopt a constant pressure, constant density sphere, we find that only the two lowest order even-parity modes couple to the tide (Papalizou & Savonije 1997).

For models satisfying a single power-law density profile ($\rho/\rho_0 = (r/R)^{-\gamma}$), $C_n \propto n^{-1} n^{2+\gamma/2}$ for even-parity modes (n is even). For instance, when $\gamma = 1.8$, $C_n \propto n^{-1.6}$. This scaling is supported by integration of both the actual inertial mode eigenfunctions and of the simple toy-model.

In models of Jupiter, gas pressure can be obtained from ideal gas law above a layer at radius $r=R-0.98$, while it is dominated by strongly interacting molecules below this layer (discussed in Appendix A.1). The model can be roughly fitted by a two power-law density profile, with varying from a value of 1.8 near the surface to 1 deeper down. This changing affects the tidal overlap. Let the transition occur over a radius r . We find $C_n \propto n^{-1}$ for $n \leq R/r$ and $C_n \propto n^{-1.6}$ for larger n values. Realistic Jupiter models presented by Guillot et al. (2004) yield $r/R \approx 0.02$, or $r \approx 4$ local pressure scale heights.

The tidal overlap is also affected by discontinuities in density or density gradient. The former occurs if the metallic hydrogen phase transition is of the first-order. For a discontinuity with a fractional value $\Delta = \Delta_0$. We have $C_n \propto (1-\Delta_0)n^{-1} = n^{-1}/(1-\Delta_0)$. A discontinuity in density gradient results if the above transition is of second-order in nature. For a fractional discontinuity of $\Delta_0 = 0$, the overlap integral $C_n \propto (1-\Delta_0)n^{-3}/(1-\Delta_0)$.

So in conclusion, the magnitude of the cancellation in

the overlap integral depends on the density profile, both its overall scaling with depth as well as its interior discontinuities and sharp changes.

It is interesting to notice that one can substitute the actual inertial mode eigenfunction with a fast-oscillating cosine function of the radius and obtain the same scalings as the ones listed here (see Fig. D10). It is as if one can almost make do without detailed knowledge of the eigenfunction. This insensitivity leads us to believe that, although we are in many cases using an approximate solution for the inertial mode eigenfunction, our results for the overlap integral is reliable (more discussion in Appendix D).

Why is it necessary to go through all these detailed analysis? In the expression for C_n , while the denominator is fairly straightforward to obtain through direct numerical integration, the severe cancellation suffered by the integral in the numerator renders the numerical results in many cases untrustworthy. For instance, a 10^{-4} inaccuracy in the Jupiter model presents itself as a small (but finite) density jump and affects strongly the value of C_n at large n .

2.3. Turbulent Dissipation

We demonstrated in Paper I that energy of an inertial mode is stored mostly in the form of kinetic energy. An inertial mode causes little compression or changes in the gravitational potential. As a result, its dissipation is dominated by shear viscosity.

The forcing by shear viscosity appears in the equation of motion as

$$+ 2 \frac{\partial}{\partial r} \left(\frac{r}{\rho} \frac{\partial \rho}{\partial r} \right) + F ; \quad (9)$$

where the viscous force

$$F = \eta \frac{\partial}{\partial r} \left(\frac{r}{\rho} \frac{\partial \rho}{\partial r} \right) ; \quad (10)$$

and η is the shear viscosity coefficient, related to the properties of convection by the following mixing length formula,

$$\eta = \frac{1}{2} \rho v_{cv} \frac{1}{1 + (\tau_{cv}/2)^s} ; \quad (11)$$

Here v_{cv} , τ_{cv} and ρ_{cv} are the characteristic convection velocity, scale length and turn-over time. The reduction coefficient s encapsulates our ignorance of the behavior of turbulent viscosity for the case that the convective turn-over time is very long compared to the tidal period. Here, we adopt $s = 2$ (see Appendix A.2); we will discuss in x4 the effects on our results when taking $s = 1$. We further define the depth ($R - r$) at which $\tau_{cv}/2 = 1$ to be z_{crit} . For the models of Jupiter models we adopt (see Appendix A.2 & Fig. A.8), $z_{crit} \approx 10^{-2.8} R$ and

$$\begin{aligned} \eta &\propto (z/R)^{-1} & \text{for } z > z_{crit}; \\ \eta &\propto 10^0 (z/R)^{-1-3} & \text{for } z < z_{crit}; \end{aligned} \quad (12)$$

Here, η is taken to be the surface value ($\eta = 1.8$). The deeper region where $\eta = 1.0$ has too weak a viscosity to be of concern.

We assume here that the viscous forcing is small compared to the restoring force for inertial modes so we can

/ $z_1^{-1} = 3$. We repeat the scaling exercise in equation (15) and obtain

$$\gamma = 1.5 + 2 = 3; \quad (18)$$

We used numerical integration to obtain damping rates for a range of power-law models, with n_1 ranging from 1.0 to 3.0. The results are presented in Fig. 1. Some of these models have double power-law density profiles but only the value at the envelope affects the scaling for the damping rates.⁹ The numerical results confirm our analytical scalings.

We have also computed damping rates using realistic models published by Guillot et al. (2004). These models are discussed in Appendix A and have $n_1 = 1.8$ in the outer envelope. The numerical results are shown in Fig. 2. They satisfy the scalings derived above and can be summarized as,

$$\begin{aligned} \gamma &= 6 \times 10^{13} \frac{1}{7.59} \omega^{7.1} \quad \text{for } \omega < 50; \\ &= 3 \times 10^9 \frac{1}{7.59} \omega^3 \quad \text{for } \omega > 50; \end{aligned} \quad (19)$$

where we have scaled γ by 7.59, the value of γ for a low order inertial mode ($n_1 = n_2 = 1$). Even this low order inertial mode is rather more strongly damped than the equilibrium tide. The transition occurring at $\omega = 50$ is caused by the fact that the upper turning point at this value coincides with $z_{\text{crit}} = 10^{2.8} R$. Moreover, while we have calculated damping rates for modes with various ($n_1; n_2$) combinations, we find that their damping rates depend only on ω .

3. tidal Q for jupiter

3.1. Equilibrium Tide Result

In equation (1) (Goldreich & Soter 1966), E_0 is the tidal energy stored in the equilibrium tide, expressed by equation (7), and the time-integration is carried out over one tidal cycle.

For the equilibrium tide, we obtain $Q_{\text{equi}} = \gamma / \omega = \gamma_{\text{equi}}$ where γ is the tidal frequency in the rotating frame ($\omega = 2\pi / T = 2\pi / (1.532 \text{ d}) = 1.532$), and γ_{equi} is the turbulent damping rate for the equilibrium tide as calculated in §2.3.1. Substituting with the value $\gamma_{\text{equi}} = 4 \times 10^{16} \text{ s}^{-1}$, we obtain $Q_{\text{equi}} = 10^{12}$, while Goldreich & Nicholson (1977) presented an estimate of $Q_{\text{equi}} = 5 \times 10^3$. Considering that their estimate is more order-of-magnitude in nature, and that the exact value of turbulent viscosity is uncertain (easily by a factor of 10), these two estimates roughly agree. In any case, the equilibrium tide, as has been argued long and hard, can not be responsible for the outward migration of Io and other satellites.

3.2. Inertial Mode Results

What Q value do inertial modes bring about? In terms of dissipating tidal energy, inertial modes are in some ways superior to the equilibrium tide. Inertial modes that can be driven by the tidal forcing are dense in the frequency range of interest (§2.1), and they are damped much more

strongly than the equilibrium tide (§2.3.2). The disadvantage, however, lies in the generally weak coupling between an inertial mode and the tidal potential. Can the first two advantages overcome the last disadvantage? Here, we combine results from previous sections to calculate the tidal Q caused by inertial modes.

3.2.1. Q value by Individual Modes

We start by calculating the amount of tidal energy dissipated via one inertial mode. The following forced-damped oscillator equation describes the interaction between an inertial eigenmode and the tidal forcing,

$$m \ddot{x} + \gamma \dot{x} + \omega_0^2 x = r_{\text{tide}} \exp(i\omega t); \quad (20)$$

where x is the displacement, and the three terms on the left-hand-side represent, respectively, the inertia, the viscous damping, and the restoring force. The free mode will have an eigenfrequency of ω_0 . The right-hand-side is the tidal forcing with frequency ω which we take to be $\omega = \omega_0$. Adopting the substitution $x = \tilde{x} e^{i\omega t}$ with the tilded quantities normalized as $\tilde{x}^2 = 2x^2$, $\tilde{\gamma} = \gamma$, multiply both sides by \tilde{x} and integrating over the planet, we obtain the amplitude

$$\tilde{x} = \frac{C}{2} \frac{e^{i\omega t}}{\frac{\omega_0^2}{\omega^2} - 1 + \frac{\tilde{\gamma}^2}{\omega^2}} = \frac{C}{2} \frac{e^{i\omega t + i}}{4(\frac{\omega_0^2}{\omega^2} + \frac{\tilde{\gamma}^2}{\omega^2})} \quad (21)$$

where the tidal coupling $C = \int d^3r \tilde{r}^0 \tilde{r}_{\text{tide}}$, the frequency detuning $\Delta = \omega - \omega_0$ ($\omega_0^2 = 2\pi^2$), and the angle $\phi = \tan^{-1}(\Delta / \tilde{\gamma})$ (we assign $\phi > 0$ for damping). For the equilibrium tide ($\omega = \omega_0$), this angle represents the lag-angle between the tidal bulge and the tide-raising body, $2 \tan^{-1}(\Delta / \tilde{\gamma}) = \phi_{\text{equi}} = 1 = Q_{\text{equi}}$ (eq. [1] & §3.1).

Energy in the inertial mode is simply \tilde{x}^2 , and the energy dissipated via this mode over one period can be found by

$$\begin{aligned} E &= \int \frac{dE}{dt} dt = \int \frac{d^3r}{dt} \text{Re}[-\text{Re}[r_{\text{tide}} e^{i\omega t}]] \\ &= \int \int \frac{d^3r}{dt} \sin(\omega t + \phi) \cos(\omega t) \\ &= \int \int \sin \phi = \frac{\phi C^2}{2(4\frac{\omega_0^2}{\omega^2} + \tilde{\gamma}^2)}; \end{aligned} \quad (22)$$

The tidal Q is related to the above quantity by eq. (1)

$$Q = \frac{2 E_0}{E} = \frac{4 E_0}{\phi C^2} \frac{4\frac{\omega_0^2}{\omega^2} + \tilde{\gamma}^2}{2}; \quad (23)$$

where again E_0 is the energy in the equilibrium tide, and the factor in the parenthesis describes the effect of being off-resonance. This expression can also be derived more simply taking $E = 2\pi \int \tilde{x}^2 d^3r$.

We call a mode "in resonance" with the tide whenever $2\pi \int \tilde{x}^2 d^3r$. The Q factor associated with a resonant mode, Q_{res} , is proportional to the dissipation rate and inversely proportional to the normalized tidal coupling,

$$Q_{\text{res}} = \frac{4 E_0}{C^2 \phi} = \frac{128}{15 \phi} \frac{R^{\frac{2}{3}} \rho^{\frac{6}{5}}}{\int \frac{1}{P} dr} \frac{\int \frac{1}{2} R^{\frac{1}{2}} d^3r}{\int \frac{1}{2} R^{\frac{1}{2}} d^3r} \frac{1}{\phi^2 \cos(2\phi)}; \quad (24)$$

⁹ For these double power-law models as well as for realistic jupiter models, the inertial mode eigenfunctions are obtained as described in Paper I.

The results are presented in Figs. 3 & 4 for the two models. As is shown in these figures, Q value fluctuates wildly as a function of the forcing frequency. While there is a ceiling to the overall Q value, there may be occasions when resonance with very low-order modes occurs, leading to deep valleys with the Q reaching values as small as 10. The ceiling, on the other hand, is determined by 60 modes which are always in resonance at any forcing frequency. Due to their high Q_{res} values, modes of orders higher than these are not important.

The results should be interpreted statistically. One can infer from them two pieces of information about Jupiter's Q value. The first is the average Q value across a certain frequency range, and the second the probability of Q value falling below 10^6 in this frequency range. Here, the value $Q = 10^6$ is taken to be the rough upper limit for the empirically inferred Q value.

The definition for the word 'average' deserves some deliberation. We follow Goodman & Oh (1997) and Terquem et al. (1998) in adopting the following average,

$$Q = \frac{\int_0^1 Q(\omega) d\omega}{\int_0^1 d\omega} \quad (32)$$

This is equivalent to a time-weighted average since the time a system spends in a certain state is inversely proportional to the torque at that state. Over the evolutionary timescale, the system quickly moves through the deep valleys (large torque) and lingers around in the large Q region. This is where we expect to find it.

We find that for $2.07; 0.8$, $Q = 1.4 \times 10^6$ for model B and $Q = 5.8 \times 10^6$ for model D, roughly consistent with our analytical estimates. Recall that $Q_{\text{equi}} = 10^{12}$. Moreover, at any forcing frequency, the probability that Jupiter has $Q < 10^6$ is 3% in model B and 10% in model D.

4. discussion

Throughout our calculation, we have assumed that Jupiter is uniformly rotating, neutrally buoyant and coreless. We have also assumed that its internal convection provides a turbulent viscosity which is quantified by the mixing length theory and which is reduced with an index $s = 2$ when the convection turn-over time is long compared to the tidal period. We obtained inertial mode eigenfunctions for realistic Jupiter models using a combination of WKB approximation and exact surface solution (Paper I).

In this section, we discuss the validity of our various assumptions, factors that might influence our results, as well as implications of our results.

4.1. Tidal Overlap

Firstly, a precaution about tidal overlap. We find that this is the trickiest part of our work because inertial modes are propagative essentially over the whole planet, with a small evanescent region very close to the surface. Regions of positive and negative tidal coupling lay side by side, leading to strong cancellation and extreme sensitivity to numerical accuracy. In fact, for a sphere with a density profile that follows a single power-law, the net tidal coupling decreases with increasing mode order so strongly

(Appendix C) that numerical precision is soon strained even for fairly low-order modes. Inertial modes are not important for tidal dissipation in these models.

In a realistic Jupiter model, the cancellation is less extreme due to the following two features: the molecular to metallic hydrogen transition at $r/R = 0.8$ (either a discrete phase transition or a continuous change) and the polytropic index change at $r/R = 0.98$ where hydrogen molecules change from ideal gas to strongly interacting Coulomb gas (discussed in Appendix A.1). These two features act as some sort of 'internal reflection' for the inertial modes (their WKB envelopes inside and outside of these features differ). This weakens the above-mentioned near-perfect cancellation in the overlap contribution from different regions and leads to larger tidal coupling. This is confirmed by integration using both a toy-model (Appendix D) and actual inertial mode eigenfunctions. In this case, tidal dissipation via inertial modes outweighs that due to the equilibrium tide.

The inertial mode eigenfunctions for realistic Jupiter models are constructed as follows (see also Paper I). We first obtain eigenfunctions for a single power-law model with the power-law index (γ) determined by that in the outer envelope of the Jupiter model. This can be done exactly as long as we ignore the Eulerian density perturbation in the equation of motion¹¹. We multiply the resulting wave-function by a factor $\frac{W}{W_{\text{surf}}}$ where W_{surf} is the density from the single power-law and W is the actual density. We showed in Paper I that in the WKB region, this construction approximates the actual eigenfunction to order $O(1 = \epsilon^2)$, and it is exact in the surface evanescent region.

The effects of such a non-exact formulation on mode eigenfrequencies will not significantly alter our results and its effects on the damping rates are negligible. But does it affect our results on tidal coupling, which, as we have shown, is a sensitive function of numerical accuracy? A definitive answer may have to come from high resolution numerical calculations. But our toy-model gives us some confidence that our approach has captured the essence of the problem and that our overlap result is qualitatively correct.

4.2. Turbulent Viscosity

The next issue concerns the turbulent viscosity. We have presented the detailed viscosity profile in Appendix A.2 & Fig. A.8.. This is calculated based on the mixing-length theory which is order-of-magnitude in nature (also see eq. [11]). How much does the Q value change when the viscosity is raised (or decreased) by a factor of, say, 100? The scaling in equation (31) yields $Q \propto \frac{1}{\rho_0^{n_Q + 2}}$. So $Q \propto \rho_0^{-0.8}$ for model B and $\propto \rho_0^{-0.5}$ for model D. So this causes a change in the Q value that is comparable to our numerical accuracy and is not significant.

Zahn (1977) has proposed an alternative expression to account for the reduction in the turbulent viscosity when the convective turn-over time is much longer than the tidal period. He advocated a less drastic reduction of $s = 1$ for the index in equation (11). This produces two differences

¹¹ This term is small and its removal from the equation of motion, as we discussed in Paper I, does not preclude tidal forcing between the tide and the inertial modes.

to our results. First, the equilibrium tidal Q is reduced to 10^0 as the effective viscosity is increased over the bulk of the planet by a factor of 10^3 . Inertial modes also in general experience stronger dissipation, with the change more striking for low-order modes. Modes of lower order can now better satisfy the resonance condition ($2j \neq j$). This would have reduced the overall Q factor but for the fact that the enhanced η means every mode now has a larger Q_{res} . Our numerical results (Fig. 5) show that the overall Q is hardly modified from the $s = 2$ case.

4.3. Phase transition

The equation of state for hydrogen at M bar level is currently uncertain. The transition from a molecular fluid to a conductive fluid (metallic hydrogen) can be either a plasma phase transition (PPT) with a discreet density jump, or a continuous process (represented by the interpolated EOS). As our results (Figs. 3 & 4) show, the overall Q factor is 10^7 in the former case and 10^0 in the latter case. This difference arises from the difference in the overlap integral. In the PPT case, cancellation in the overlap contribution coming from different parts of the planet is less severe ($C_n / 1 = n^2$), while it is more complete in the interpolated EOS case ($C_n / 1 = n^3$). This difference is explained by a toy model in Appendix D.

In the case of a first-order PPT, our result is not sensitive to the location of the phase transition, as long as it is not within, say, 10% radius of Jupiter. This feature in our theory is useful for understanding tidal dissipation in extra-solar Jupiters as they likely have their PPT at different radii from that of Jupiter.

The $C_n / 1 = n^3$ scaling in the interpolated EOS case can be attributed to two factors. If the phase transition is second-order in nature, there will be a discontinuity in density gradient. This will lead to the above scaling. Another factor that can contribute similarly, is that the polytropic index γ_1 (or, equivalently, the power-law index γ) has a sharp transition at $r = R_{0.98}$, spanning a range of $r = R_{0.02}$, or 4 local pressure scale heights (Appendix A.1). The overall Q factor is little affected if either transition region is shifted upward or downward by a few pressure scale heights. However, if the second-order phase transition does not exist, and if the polytropic transition occurring over a range $r = R_{0.02}$, we expect $C_n / 1 = n^{4.6}$ and the overall Q factor to be much larger.

Our Q value calculations favor models with a first-order phase transition. This has interesting implication for the formation of Jupiter. Guillot et al. (2004) showed that among models that match all observational constraints on Jupiter, the ones with PPT equation of state have larger core mass and lower total mass of heavy elements, while the ones with interpolated equation of state tend to the opposite.

4.4. The presence of a Solid Core

We have assumed here that convection penetrates into the center of Jupiter. If Jupiter does have a solid core, inertial modes are excluded from the central region. What is the effect on the tidal Q factor?

Demott (1979) pointed out that body tide in the (imperfectly elastic) solid core of Jupiter with a core quality factor $Q \sim 30$ can account for the observed tidal dissipa-

tion. However, this requires a core size which is at the upper-end of current determinations ($r_{\text{core}} = R_{0.15}$) as well as a core quality factor which is currently unknown. Here we restrict ourselves to consider the effect of core on inertial modes.

For an estimate, we retain the inertial mode eigenfunctions calculated for the core-less case, but suppress the contribution from the core region to mode energy, mode damping, and tidal overlap integral. We find no substantial difference from the a core-less case (one can also compare results from model B which is core-less and model D which has a $10M_{\oplus}$ core). Contribution from the core region to the overlap integral, for instance, is insignificant as the radial integrand drops as $1/r^6$ (eq. [C3]): this is partly due to the radial dependence of the tidal potential ($1/r^2$), and partly due to the more anelastic nature of the inertial modes (small Q) in the high density region.

A more subtle influence of the core, however, may be present. While we have been able to separate spatial variables and calculate inertial mode eigenfunctions in the ellipsoidal coordinates for core-less models, the presence of a spherical core destroys this convenience. The inner boundary conditions can no longer be defined along constant ellipsoidal coordinate curves and we have to return to the original partial differential equations. This is analogous to the situation where the Coriolis force breaks the symmetry of a spherical star, with the result that the angular dependence of an eigenmode in a rotating star can no longer be described by a single spherical harmonic but only by a mixture of them. So it is perceivable that if we adopt core-less inertial mode eigenfunctions as a complete basis, inertial mode eigenfunction in the presence of a spherical core may be a mixture of these functions. This gives us a hint on how to proceed when there is a core. It is possible to obtain the mixing ratio and use these to calculate new damping rates, mode energy and tidal coupling. We conjecture that the mixture becomes purer (more dominated by one component) as the core size approaches zero. In particular, we expect the mixing not to be important when the core size is much smaller than a wavelength of the inertial mode ($r_{\text{core}} = R_{0.1} =$). We plan to extend our calculation to the solid core case in the future.

The above conjecture seems to be supported by numerical calculations by Ogilvie (private communication) when he decreases the core size and recovers low-order inertial modes. When the core size is significant, however, O'L's study discovered something else. Instead of global inertial modes, they found that fluid response to the tidal forcing is concentrated into characteristic rays which become singularly narrow as viscosity goes to zero. This appears a rather different picture from ours and it is imperative to understand the physical origin of these singular rays.

4.5. Radiative Atmosphere

We have also assumed that the convection zone extends all the way to zero density. This may be unrealistic for Jupiter, and worse still for exo-jupiters. In the Jupiter models we adopted, convection gives way to radiation just above the photosphere. It is possible that an inertial mode can find itself in resonance with a gravity mode and smudge some wave-ux out of the convective region. The Brunt-Vaisala buoyancy frequency there can be roughly

estimated from the local sound speed as

$$N = \frac{g}{c_s} \frac{2700}{9.3e4} = 0.029 \text{ s}^{-1}; \quad (33)$$

which is much higher than the inertial-mode frequencies we are interested in ($\sim 3.5 \cdot 10^4 \text{ s}^{-1}$). So the gravity-mode will have to be high-order and rotationally-modified, satisfying $N \ll 1$. Such modes can be obtained (semi-)analytically under the 'traditional approximation' and are called the 'Hough modes'. The smuggled waveflux is subsequently lost in the higher atmosphere where the gravity-wave breaks. This brings about enhanced damping to the inertial-mode. Recall that the overall Q factor scales roughly as inverse square root of the damping rate. So unless the resultant damping rate is orders of magnitude above the rate of turbulent damping, the overall Q factor is little affected.

There are other ways in which a radiative envelope may affect inertial-modes. The upper-turning point ($z=R_1=2$ when $\cos^2 \theta = 1$ and $z=R_1=0$ otherwise) of a sufficiently high order inertial-mode may fall near or above the convective-radiative interface. When this occurs, the structure of the inertial-mode is significantly modified. The radiative region imposes a different surface boundary condition on the inertial-mode than the one we assume here (vanishing Lagrangian pressure perturbation). This different boundary condition, as is illustrated by the toy model in Appendix D, may give rise to much different (likely larger) tidal overlap and therefore a different Q (likely smaller) factor (see also x4.7).

Extra-solar hot Jupiters are strongly irradiated by their host stars. Their atmosphere is more isothermal leading to a substantially thicker radiative envelope (down to 30 km below photosphere) than that in Jupiter. This envelope may sustain rotationally-modified gravity-waves ('Hough Modes') which may be resonantly (if these waves are trapped) excited by the tidal potential. It is possible that this explains the tidal dissipation in these hot Jupiters (Lubow et al. 1997). However, inertial-modes should still exist and will couple to the tidal potential even in these planets. The fact that the Q -values appear to be similar between the exo-Jupiters and our Jupiter leads us to suspect that inertial-modes will remain relevant.

4.6. Where is the tidal energy dissipated?

In our picture of resonant inertial-mode tide, most of the tidal dissipation occurs very near the surface, where both the kinematic viscosity and the velocity shear are the largest. In a realistic Jupiter model, the effective turbulent viscosity peaks at a depth of 60 km (z_{crit} , Fig. A8 in Appendix A 2), and decays sharply inward. Meanwhile, the displacement caused by inertial-modes rises outward toward the outer turning point. And the velocity shear reaches its maximum inside the 'singularity belt' (Paper I), which is found to be around $\cos^2 \theta = 1$, with an angular extent $R = 1$ and a depth $R = 2$. For inertial-modes most relevant for tidal dissipation ($j \sim 60$), this depth roughly coincides with the location of maximum viscosity. We have confirmed numerically that most of the dissipation indeed occur in this shallow belt.

The tidal luminosity in Jupiter is $7 \cdot 10^{20} (10^6 = Q) \text{ erg/s}$. What is the effect of depositing this much energy in a shallow layer? We compare this against intrinsic Jovian flux of $F \sim 5000 \text{ erg/cm}^2 \text{ s}$. The total intrinsic luminosity passing through the belt is $2 \cdot R^2 = F \cdot 3 \cdot 10^2 \text{ erg/s}$. This is larger (or at worst comparable) to the tidal luminosity. Another way of phrasing this is to say that the local thermal timescale is shorter (or at worst comparable) to the local thermal energy divided by the tidal flux. So the belt is expected to be able to get rid of the tidal energy without suffering significant modification to its structure.

Angular momentum is also deposited locally. We assume here that the convection zone is able to dissipate the excess angular momentum almost instantaneously toward the rest of the planet. However, if convective transport is highly anisotropic and prohibits diffusion, it is possible that this (negative) angular momentum is shored up near the surface and contributes to surface meteorology of Jupiter.

The transiting planet HD 209458b is observed to have a radius of $1.3 R_J$ (Brown et al. 2001). Its proximity to its host star and its currently near-circular orbit raise the possibility that its over-size is a result of (past or current) tidal dissipation (Gu et al. 2003). However, if our theory applies also to these hot-Jupiters, we would expect that the tidal heat is deposited so close to the planet surface that it can not be responsible for inflating the planet.¹² The higher intrinsic luminosity of hot Jupiters implies larger turbulent viscosity, with the result that inertial-modes satisfying $2j \ll j_{\text{crit}}$ may be slightly lower in order than those in Jupiter (~ 60). For these planets, tidal luminosity is of order $10^{26} (10^6 = Q) \text{ erg/s}$, while the intrinsic luminosity passing through the singularity belt is $7 \cdot 10^6 \text{ erg/s} (T_e = 1000 \text{ K})^4$. So again, tidal luminosity is not expected to substantially alter the structure of the upper layer. Moreover, given the short local thermal timescale, any change to the planet structure should disappear once tidal dissipation ceases.

If inertial-modes are resonantly excited to large amplitudes, it is foreseeable that they can force other inertial-modes in the planet and be dissipated by nonlinear coupling. To see whether this is important, we consider the amplitude of inertial-modes. This is largest near the surface around the 'singularity belt'. When an inertial-mode is resonantly excited ($j \sim j_{\text{crit}}$), we obtain a horizontal surface displacement $\eta \sim 10^1 (=7.59) \cdot 10^7 \text{ cm}$. While this implies extreme amplitudes for low-order modes, they only come into resonance rarely. For modes of interest ($j \sim 60$), the typical surface displacement amplitude is $10^3 \text{ cm} \sim 10^{-7} R_J$.¹³ So, nonlinear effects are likely unimportant for inertial-modes.

4.7. Comparison with Ogilvie & Lin (2004)

The most relevant work to compare our results against is that of OL, which is an independent study that appeared while we were revising our paper. In their work, the same physical picture as that discussed here was considered, namely, tidal dissipation in a rotating planet. They

¹² It is difficult to imagine how entropy deposited near the surface can be advected inward to raise the entropy level of the entire planet.

¹³ In contrast, the displacement amplitude of the equilibrium tide is 60 m. The extremely weak dissipation of the equilibrium tide is responsible for their large Q_{equi} .

employed a spectral method to solve the 2-D partial differential equations which describe fluid motion forced by the tidal potential inside a viscous, anelastic, neutrally buoyant, polytropic fluid. This procedure directly yields the value of the tidal torque on the planet, without going through a normal mode analysis. The numerical approach allows them to include the effect of a solid core, as well as that of a radiative envelope. Overall, they concluded that inertial waves can provide an efficient mechanism for tidal dissipation, and that the tidal Q factor is an erratic function of the forcing frequency. We concur with these major conclusions.

However, many technical differences exist between the two works. To better understand both works, it is illuminating to discuss some of these differences here.

Firstly, as is mentioned in §4.4, while we obtain global inertial modes which have well defined WKB properties and discrete frequencies, OLL demonstrated that the tidally-forced response of a planet is concentrated into characteristic rays which are singular lines in the limit of zero viscosity. While viscous dissipation in their case occurs in regions harboring these rays, our inertial modes are predominantly dissipated very near the surface (the ‘singularity belt’). Moreover, although both our Q values exhibit large fluctuations as a function of tidal frequency, the origin of the two may be different { in our case, a deep valley indicates a good resonance between the tide and a low-order inertial mode, while the situation is less clear in their case. All these differences may originate from the presence (absence) of a solid core in their (our) study. We are currently investigating the underlying mathematical explanation for these differences. Again, it is interesting to note that as the core size approaches zero, inertial modes seem to reappear (Ogilvie, 2004, private communication).

Secondly, OLL’s results are based on a $n = 1$ polytrope, for which we find that tidal coupling is vanishingly small (see Appendix C),¹⁴ and that inertial modes are not important for tidal dissipation. It is currently unclear whether this difference arises from the presence of a core or from the presence of a radiative envelope in their study. Despite a steep suppression of the tidal overlap integrand near the center (integrand $\propto r^6$), the presence of a solid core may affect tidal overlap in a more substantial manner by reflecting inertial waves and changing their mode structure (§4.4). Meanwhile, a surface boundary condition specified at a finite density (instead of at $\rho = 0$) may cause extra tidal coupling (§4.5), as is shown by the analysis in Appendix C. This issue is likely unimportant for Jupiter but more relevant for extra-solar hot-jupiters which have deeper radiative envelopes.

Thirdly, OLL assumed a constant Ekman number throughout the entire planet. Since

$$Ek = \frac{\nu}{\Omega R^2} = \frac{\nu}{\Omega R^2}; \quad (34)$$

this implies that the effective viscosity $\nu = \Omega R^2 Ek$. $2 \times 10^6 Ek$ is constant throughout the planet. We have argued that the effective viscosity value for the equilibrium tide should be of order $10^6 \text{ cm}^2 \text{ s}^{-1}$ (§2.3.1), or an effective $Ek \sim 10^{13}$. However, such a weak viscosity is much smaller than is currently reachable by a numerical

method in a reasonable amount of time. Instead, OLL have opted for an alternative treatment in which they steadily decreased the Ekman number from $Ek = 10^{-4}$ to 10^{-7} and argued (based both on numerical evidence and on an analytical toy model) that the final Q value is independent of the Ekman number. This contrasts with our results that Q roughly scales as $\nu_0^{1/2}$ (§4.2) for realistic viscosity profiles, where ν_0 is the damping rate for a mode of wavenumber ν_0 .

To make the comparison more appropriate, we adopt a constant viscosity inside the planet and find that mode damping rates $\gamma = 5 \times 10^9 (Ek = 10^{-7}) (7.59)^{3/2} \text{ s}^{-1}$ in the Jupiter model D. Applying scalings derived in §3.2.1, we find $Q \sim 2.3 \times 10^6 (Ek = 10^{-7})^{-1}$. The individual mode Q_{res} value also scales inversely with the Ekman number, different from the case with realistic viscosity profile. These values are consistent with those obtained by OLL at $Ek = 10^{-7}$. Meanwhile, the equilibrium tide gives rise to $Q_{\text{equi}} \sim 4 \times 10^6 (Ek = 10^{-7})^{-1}$. So in models of a constant Ekman number, inertial modes contribute comparably to tidal dissipation as does the equilibrium tide. These results are presented in Fig. 6.

5. summary

In a series of two papers (Paper I & this), we have examined the physical picture of tidal dissipation via resonant inertial modes. This applies to a neutrally-buoyant rotating object in which the tidal frequency in the rotating frame is less than twice the rotation frequency.

In Paper I, we first demonstrate that under some circumstances (power-law density profiles), the partial differential equations governing inertial modes can be separated into two spatial dimensions and their eigenfunctions can be obtained semi-analytically. We also show that this method can be applied more generally to spheres of other density profiles, with the price that the solution is exact in the surface region but approximate in the WKB regime. Nevertheless, this approximate solution allows us to draw many physical conclusions about inertial modes, as well as about their interactions with both the tidal potential and the convection. This semi-analytical technique gives us an edge over current computational capabilities, though full confirmation of our conclusions may require careful and high-resolution numerical approaches. It is clear from our study that any numerical approach would need to sufficiently resolve the so-called ‘singularity belt’ near the surface where the inertial modes vary sharply, and that a numerical approach needs to be very cautious when evaluating the tidal overlap.

In this paper, we discuss the rate of tidal dissipation brought by inertial modes. This depends on the following three parameters: how well coupled an inertial mode is to the tidal potential, how strongly dissipated an inertial mode is by the turbulent viscosity, and how densely distributed in frequency are the inertial modes. We have obtained all three parameters using both toy models as well as realistic Jupiter models. Low-order inertial modes, if in resonance ($\nu < \gamma$, where ν is the typical frequency detuning between the tidal frequency and the mode frequency, γ the mode damping rate), can dissipate tidal en-

¹⁴ Although we only present results for a $n = 1$ power-law model, they apply to a $n = 1$ polytrope as well since the two behave similarly near the surface and the core.

ergy with Q as small as $Q = 10$. However, such a resonance is rare and short-lived. Inertial modes most relevant for tidal dissipation are those satisfying $\omega = \omega_{\text{inertial}}$, where ω_{inertial} decreases with mode wave-number as $\omega_{\text{inertial}} \propto 1/n^2$. For any tidal frequency, there can be a resonance with one of these modes. These are inertial modes with wave-numbers $n = 60$ (or total number of nodes $n = n_1 + n_2 = 30$).

For Jupiter models that do not involve a first-order phase transition (hydrogen molecular-metallic transition), yet contain either (both) a second-order phase transition or (and) a sufficiently sharp change in the adiabatic index near the surface (hydrogen ideal-gas to Coulomb gas transition), we find that the averaged Q value produced by resonant inertial modes are 10^6 , much smaller than the equilibrium tide value of $Q_{\text{equi}} = 10^7$. Meanwhile, a first-order phase transition inside Jupiter brings about a density discontinuity. This boosts the tidal overlap and further reduces the averaged Q value to 10^5 , with a 10% chance that the current Q value is between 10^5 and 10^6 (the empirically inferred Q range for Jupiter). Our results are uncertain up to perhaps, one order of magnitude. But it is already clear that inertial modes cause much stronger dissipation than the equilibrium tide.

The surface movement of inertial modes is predominantly horizontal. For inertial modes that are most relevant for tidal dissipation ($n = 60$), the surface displacement amplitude $\sim 10^3$ cm. Such a small value implies that nonlinear effects are likely not important.

In our study, we have adopted the Goldreich & Keeley (1977) prescription ($s = 2$) to account for the reduction in turbulent viscosity when the convective turn-over time is long relative to the forcing period. We find that calculations adopting Zahn's prescription ($s = 1$) produce no difference in the Q value caused by inertial modes, though the equilibrium tide is significantly more strongly damped.

We do not find that our conclusion is much altered when

we include or exclude an inner core with a size that is compatible with current constraints. However, this is assuming that global inertial modes still exist in the presence of a solid core. Ogilvie & Lin (2004)'s study have revealed a new kind of fluid motion when the core is present: they found that fluid motion is tightly squeezed into 'characteristic rays' which becomes singular when the viscosity goes to zero. This is a totally different picture than the global eigenmode picture we describe here and may lead to different Q factors in models with and without core. The physical and mathematical reasons behind this difference deserve further attention.

In our theory, tidal heat is deposited extremely close to the planet surface (inside the 'singularity belt') and can be lost quickly to the outside. For Jupiter, the tidal luminosity in this region is smaller (or at worst comparable) to the intrinsic luminosity and so would not much alter the structure. However, there remains the intriguing possibility that the negative angular momentum deposited to the belt may affect surface meteorology (jet streams and anticyclones). Moreover, if this theory also applies to hot exo-jupiters, the tidal luminosity is unlikely to be responsible for inflating planets and solve the size-problem of close-in Jupiters.

Our study was stimulated by the fact that exo-solar planets exhibit similar Q values as Jupiter does. It is therefore our plan to extend the current study to exo-jupiters. It is also possible that the theory developed here has implications for Saturn, Uranus, solar-type binaries, M-dwarfs and brown-dwarfs.

Phil Arras has contributed to the early stages of this work. I thank him for an enjoyable collaboration. I also acknowledge stimulating conversations with Gordon Ogilvie and Doug Lin, and thank Tristan Guillot for making his Jupiter models publicly available.

REFERENCES

- Brown, T. M., Charbonneau, D., Gilliland, R. L., Noyes, R. W., & Burrows, A. 2001, *ApJ*, 552, 699
 Bryan, G. H. 1889, *Philos. Trans. R. Soc. London*, A 180, 187
 Demott, S. F. 1979, *Icarus*, 37, 310
 Goldreich, P. & Keeley, D. A. 1977, *ApJ*, 211, 934
 Goldreich, P. & Nicholson, P. D. 1977, *Icarus*, 30, 301
 Goldreich, P. & Soter, S. 1966, *Icarus*, 5, 375
 Goodman, J. & Oh, S. P. 1997, *ApJ*, 486, 403
 Gu, P., Lin, D. N. C., & Bodenheimer, P. H. 2003, *ApJ*, 588, 509
 Guillot, T., Stevenson, D., Hubbard, W., & Saumon, D. 2004, in *Jupiter eds. Bagenal et al.*, in press
 Hut, P. 1981, *A & A*, 99, 126
 Ioannou, P. J. & Lindzen, R. S. 1993, *ApJ*, 406, 266
 Lubow, S. H., Tout, C. A., & Livio, M. 1997, *ApJ*, 484, 866
 Mathieu, R. D., Meibom, S., & Dolan, C. J. 2004, *ApJ*, 602, L121
 Ogilvie, G. I. & Lin, D. N. C. 2004, *ApJ*, 610, 477
 Papaloizou, J. C. B. & Savonije, G. J. 1997, *MNRAS*, 291, 651
 Peale, S. J. & Greenberg, R. J. 1980, in *Lunar and Planetary Institute Conference Abstracts*, 871/873
 Ross, M., Ree, F. H., & Young, D. A. 1983, *J. Chem. Physics*, 79, 1487
 Saumon, D., Chabrier, G., & van Horn, H. M. 1995, *ApJS*, 99, 713
 Savonije, G. J., Papaloizou, J. C. B., & Albers, F. 1995, *MNRAS*, 277, 471
 Stevenson, D. J. 1978, in *Origin of the Solar System*, 395/431
 Stevenson, D. J. 1982, *Annual Review of Earth and Planetary Sciences*, 10, 257
 |. 1983, *J. Geophys. Res.*, 88, 2445
 Terquem, C., Papaloizou, J. C. B., Nelson, R. P., & Lin, D. N. C. 1998, *ApJ*, 502, 788
 Wu, Y. 2003, in *ASP Conf. Ser. 294: Scientific Frontiers in Research on Extrasolar Planets*, 213/216
 Wu, Y. 2004, *ApJ*, submitted (Paper I)
 Wu, Y. & Murray, N. 2003, *ApJ*, 589, 605
 Zahn, J.-P. 1977, *A & A*, 57, 383

APPENDIX

a. relevant properties in a jupiter model

Here, we study properties of Jupiter that are relevant for the tidal process. This is based on publicly available models of Jupiter presented in Guillot et al. (2004). They are produced with the newest equation of state and opacity calculations, including the effect of hydrogen phase transition, and alkali metal opacity. They satisfy gravity measurements (esp. J_2 & J_4) to much better than a percent and reproduce other global properties of Jupiter (radius, surface temperature, intrinsic

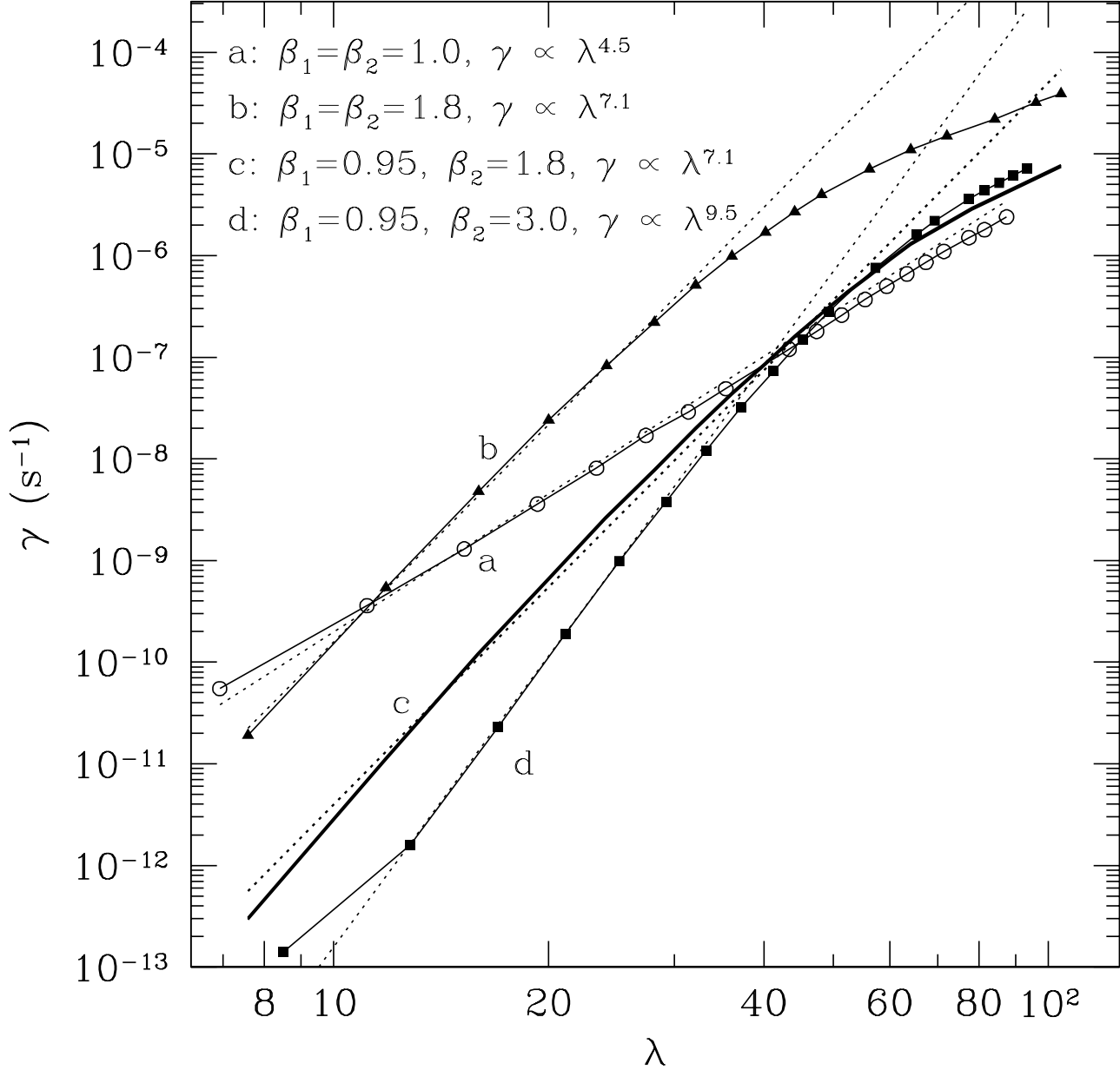


Fig. 1. Numerically computed turbulent damping rates for inertial modes in various power-law models, as a function of the mode wavenumber λ . Here, we have taken the reduction number $s = 2$ and included damping rates only for modes with $n_1 = n_2$, though other modes satisfy the same scalings observed here. Models a & b are single power-law models, while c & d are double power-law models (β_1 the index in the interior and β_2 that in the envelope) with the transition of β occurring around $r/R = 0.98$. All models are normalized to have the same central density and their viscosity profiles are described by equations (A2)–(A3). The dotted lines are power-law fits to the numerical results with the numerical scalings summarized in the top-left corner. These are well reproduced by our analytically derived relation $\gamma / \lambda^{3.5+2\beta_2}$ (eq. [17]). Notice that only the envelope power-law index enters the relation. Damping rates in all models attenuate at large λ , and scale with λ roughly as λ^3 (eq. [18]).

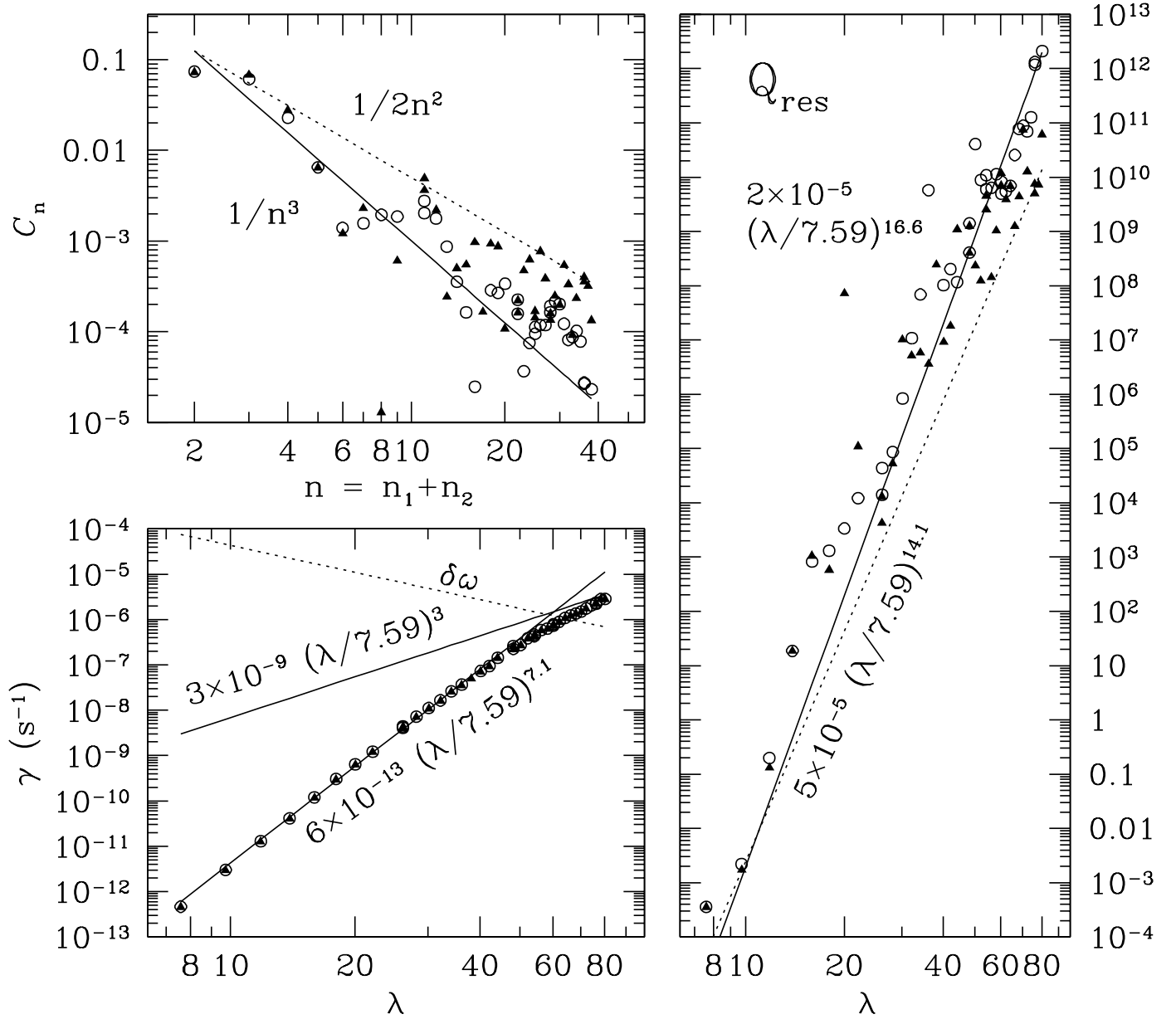


Fig. 2. Tidal coupling, viscous damping rate and resonant Q_{res} factor for various inertial-modes calculated using two Jupiter models. Model B (open circles) has no heavy metal core and no first-order metallic hydrogen phase transition, while model D (solid triangles) has a core as well as a density jump at $r=R/0.8$ due to the plasma phase transition. The upper-left panel presents the (normalized) coupling integral C_n (eq. [8]) as a function of inertial-mode node numbers ($n = n_1 + n_2$). Although the scatter is large, model B results are best fit by $C_n \propto 1/n^3$ (solid line), while model D results follow $C_n \propto 1/2n^2$ (dotted line). The lower-left panel shows the energy damping rate as a function of mode wavenumber ($\lambda = 2n$). Results from both models scale as $\lambda^{-7.1}$ for low-order modes and as λ^{-3} for high-order modes (two solid lines), consistent with analytical expectations (eq. 3.2). The dotted line in the same panel is the minimum frequency detuning as a function of λ (eq. [2]). Q_{res} , the Q value contributed by each mode when it is in resonance with the tide (eq. [24]), is plotted on the right-hand panel as a function of λ . A gain, analytical expectations for models B & D are depicted by the solid and dotted lines, respectively. Here, we have included only inertial-modes with $\lambda < 0.776$ but the results remain similar for other inertial-modes.

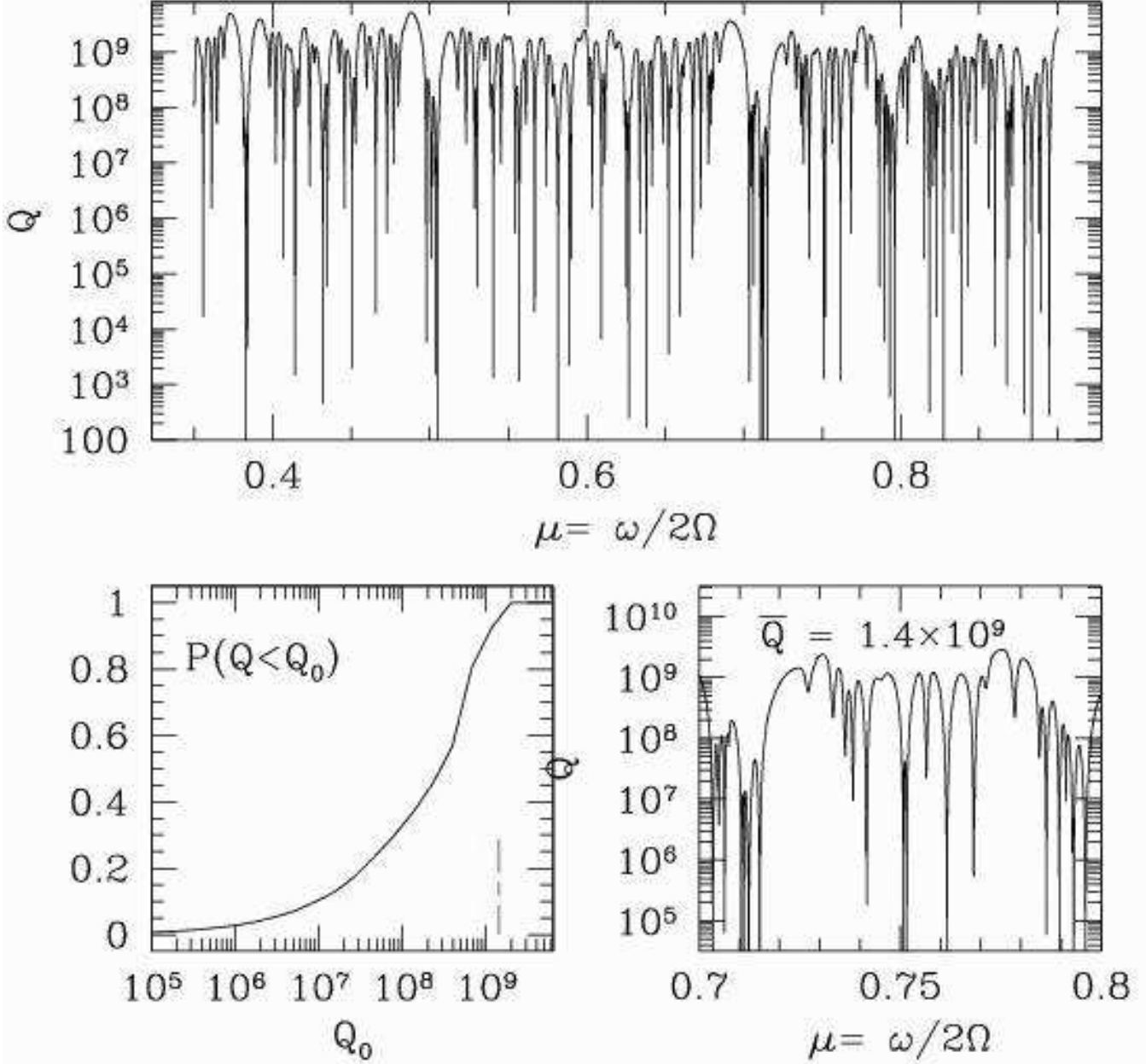


Fig. 3. Numerically calculated values of Q for model B. The upper panel shows Q as a function of the tidal frequency in the rotating frame. Deep dips occur whenever the tide is in resonance with a low-order inertial-m mode ($m = 60$), and the ceiling to the Q value is determined by the group of m modes with $m = 60$ which satisfy $2j \neq j$. The tide is always in resonance with one of these m modes at any frequency. The lower left panel shows the cumulative probability distribution of the Q value within the frequency range $0.7 < \mu < 0.8$. For a given frequency, there is 3 percent chance that we will find $Q < 10^6$. The dashed vertical curve locates the time-weighted average Q value (\bar{Q} , eq. [32]). We find $\bar{Q} = 1.4 \times 10^9$ within this frequency range. The lower right panel expands the view of the upper panel over this frequency range. The locations of the fine structure in this plot are not to be taken literally as we have adopted an approximate dispersion relation for the inertial-m modes.

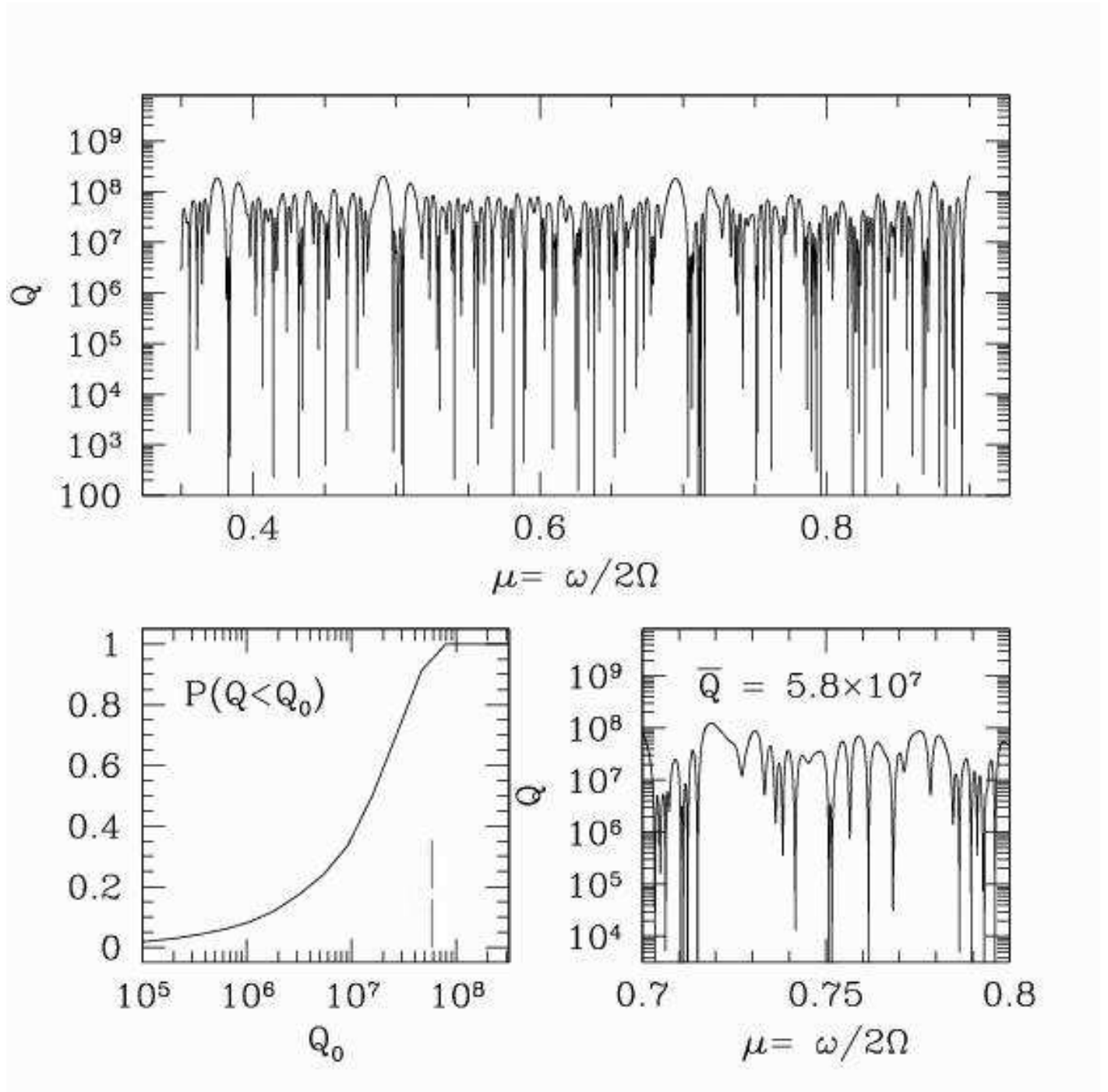


Fig. 4. Same to Fig. 3, but for model D in which the tidal coupling decreases as $1=2n^2$ as opposed to $1=n^3$. This is related to the presence of a first-order phase transition at $r=R=0.8$. While showing overall similar characteristics as those in Fig. 3, Q has now been reduced to 5.8×10^7 between $\mu = 0.7$ and 0.8 , and for any given frequency, there is a 10% chance that Jupiter exhibits $Q < 10^6$.

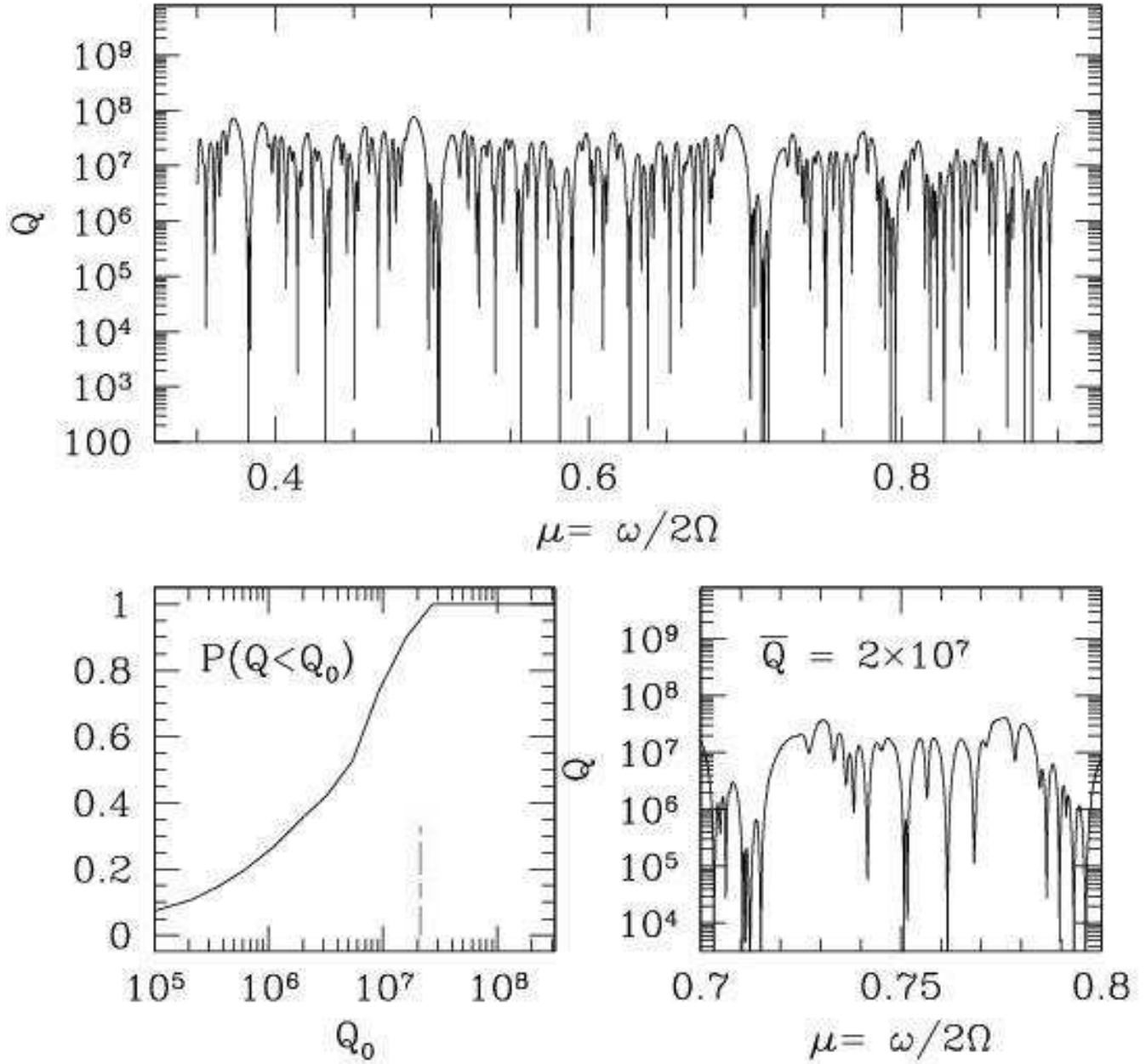


Fig. 5. Same as Fig. 4, but calculated for model D when the index for viscosity reduction is taken to be $s = 1$ (Zahn 1977) instead of $s = 2$. Mode damping rates now behave as $\gamma = 10^{-10} (\approx 7.59)^{4.5} \text{ s}^{-1}$. We obtain $Q \approx 2 \times 10^7$, with 30% chance that $Q < 10^6$ for the current tidal frequency. Moreover, $Q_{\text{equi}} = 10^6$ in this case.

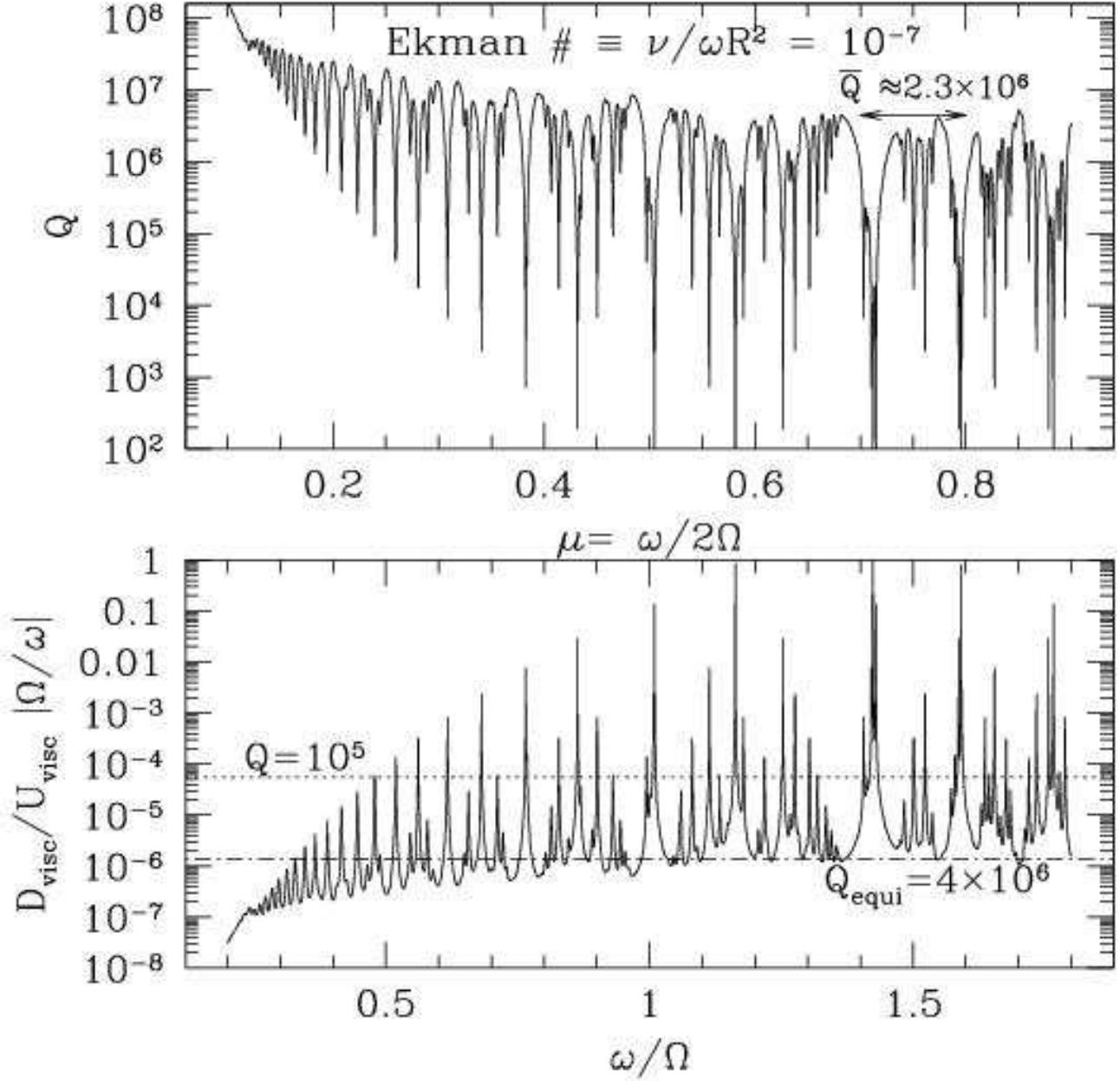


Fig. 6. We repeat our calculation for model D, taking the turbulent viscosity to be a constant throughout the planet with the Ekman number $\text{Ek} = \nu/\omega R^2 = 10^{-7}$. Mode damping rates scale much less steeply with inertial-mode wave-numbers, $\nu = 5 \times 10^{-9} \text{ (}=7.59\text{)}^{3/2} \text{ s}^{-1}$. The resulting Q value from inertial-modes is plotted against μ in the upper panel, with $Q \approx 2.3 \times 10^6$ over the range $\mu \in [0.7; 0.8]$. A similar calculation for model B yields $Q \approx 3.5 \times 10^6$. We find that the Q value is inversely proportional to the Ekman number. The lower panel translates the Q result into a quantity used in Fig. A2 of O L (the dimensionless viscous dissipation rate, $D_{\text{visc}}/U_{\text{visc}} |\Omega/\omega|$), plotted here as a function of ω/Ω . The two overlaid lines with $Q = 10^5$ (dotted) and $Q = 4 \times 10^6$ (dot-dashed), respectively represent the empirically inferred Q value for Jupiter and the Q value associated with the equilibrium tide in this model. These results resemble those presented in Fig. A2 of O L for the same Ekman number.

In this study, we focus on two models, B and D, out of the five sample models presented in Guillot et al. (2004). Model B is produced with an interpolated hydrogen equation of state (meaning no first-order metallic hydrogen phase transition), and has no heavy metal core. Model D, in contrast, contains a first-order phase transition (PPT equation of state) and has a core with mass $10M_{\oplus}$. The photosphere for both these models is located at a radius of 7.1θ cm, at a pressure of $1\theta^6$ dyne/cm², and with a temperature 170 K and a density 1.6×10^{-4} g/cm³.

The interiors of these models are fully convective (outside the core). Due to the high density in Jupiter (mean density 1.3 g/cm³), the convection speed needed to carry the small intrinsic flux (5.4×10^3 erg/s/cm²) is highly subsonic, resulting in an almost exactly adiabatic temperature profile (super-adiabatic gradient 10^{-8} or smaller). This justifies our assumption of neutrally buoyant fluid when investigating inertial modes. Only the thin atmosphere above the photosphere, with a local pressure scale height ~ 20 km, is radiative.

A.1. Density Profile

Two features in the density profile of these models deserve attention.

At radius $r=R-0.8$, pressure $1\theta^2$ dyne/cm², and density 1 g/cm³, hydrogen undergoes a phase transition. Above this layer, hydrogen is mostly neutral and molecular. Below this layer, the mean atomic spacing becomes smaller than a Bohr radius and electrons are pressure ionized. The strong Coulomb interaction and electron degeneracy resemble those in a metal and the transition is referred to as 'liquid metallic hydrogen' transition (Guillot et al. 2004). The nature of this transition is still poorly understood. Model B assumes this transition is of second-order and entails a discontinuity only in the gradient of density (of order 50%), while model D assumes it is a first-order transition with a density jump of order 10%. These two different treatments should bracket the actual equation of state of hydrogen.

Another feature sets in nearer the surface, at radius $r=R-0.98$, pressure $1\theta^0$ dyne/cm² and density 0.1 g/cm³. Above this region, the gas can be considered as ideal diatomic gas (H_2). As the temperature is below 2000 K, the mean degree of freedom for each molecule is 5 (three translational plus two rotational).¹⁵ The specific heat per molecule at constant volume and constant pressure are, respectively, $C_V = 5/2 k_B$, $C_P = 7/2 k_B$, yielding $\gamma = C_P/C_V = 1.4$. Below this region, however, γ rises to $1.8-2.2$ in the main body of the planet, and approaches 3 in the very deep interior (Stevenson 1978, 1982).

This results in different density profiles above and below this region. Recall our definition of $\rho = \rho(r)/\rho(R)$. The Jupiter models show that $\rho \sim 1.8$ (corresponding to $\gamma = 1.4$) above this layer, while $\rho \sim 1$ (corresponding to $\gamma = 2$) in the interior. We also observe that this transition of ρ occurs over a fairly narrow region of radial extent $r - R \sim 0.02R$, or 4 local pressure scale height. As is discussed in §2.2.2, this transition is of significance to our tidal coupling scenario.

But what is the cause behind the rise of γ near $p = 1\theta^0$ dyne/cm²? The ionization fraction of electron is too low ($\sim 10^{-6}$) in this region to make a difference by degeneracy pressure; hydrogen is bound into H_2 and only starts to be dissociated near $p = 1\theta^2$ dyne/cm². The true cause, it turns out, is the non-ideal behavior of molecules, a little-talked about effect. At a density of 0.1 g/cm³, the mean molecular spacing is ~ 2 Å. While the interaction potential between H_2 and H_2 molecules is mildly attractive at spacing > 3 Å (the van der Waals force), it rises exponentially inward. By the time the spacing decreases to below ~ 2 Å, this potential is more positive than $k_B T$ and the gas pressure is no longer dominated by thermal pressure, but is dominated by the repulsive interaction between molecules. This is illustrated in Fig. A7. As density rises, molecules increasingly resemble hard spheres, leading to a steeper dependence of pressure on density, or $\gamma \sim 2$ ($\gamma = 1$). This non-ideal effect loses out at $p = 1\theta^2$ dyne/cm² above which H_2 molecules are dissociated and electrons are pressure ionized (the metallic hydrogen phase).

A.2. Turbulent Viscosity Profile

Inside Jupiter, molecular viscosity is too weak to cause any discernible dissipation on the inertial modes. We turn to turbulent viscosity.

The kinematic shear viscosity is estimated from the mixing length theory as (Goldreich & Keeley 1977; Zahn 1977; Terquem et al. 1998)

$$\nu_T = v_{cv} \lambda_{cv} \frac{1}{1 + (\lambda_{cv}/2)^s}; \quad (A1)$$

where v_{cv} , λ_{cv} and τ_{cv} are characteristic convection velocity, scale length and turn-over time. The exponent s describes the reduction in efficiency when convection is slow compared to the tidal period ($\lambda_{cv} \ll 1$). Its value is still under debate, but simple physical arguments (Goldreich & Nicholson 1977; Goodman & Oh 1997) have suggested that $s = 2$, while Zahn (1977) advocated for a less severe reduction with $s = 1$. We adopt $s = 2$ in our main study but discuss the scenario when $s = 1$. Some previous studies have adopted a form without 2 in the above expression. The viscosity is effectively smaller but we will show that this does not affect the final Q -value significantly.

In mixing length theory, $v_{cv} = (u_x)^{1/3}$, $\lambda_{cv} = v_{cv} \tau_{cv}$, and $\tau_{cv} = H/\omega z$, where H is the density scale height, z is the physical depth ($z = R - r$), and ω appears in the density power-law as $\rho = \rho(R) (r/R)^{-\omega}$ for $z \ll R$. Let the depth at which $\lambda_{cv} = 2$ be z_{crit} . Above z_{crit} , ν_T depends on z weakly,

$$\nu_T \propto z^{-1/3}; \quad (A2)$$

¹⁵ This number is smaller near the photosphere when the temperature cools toward the rotational temperature of H_2 (85 K). Not all rotational levels are populated (Saumon et al. 1995).

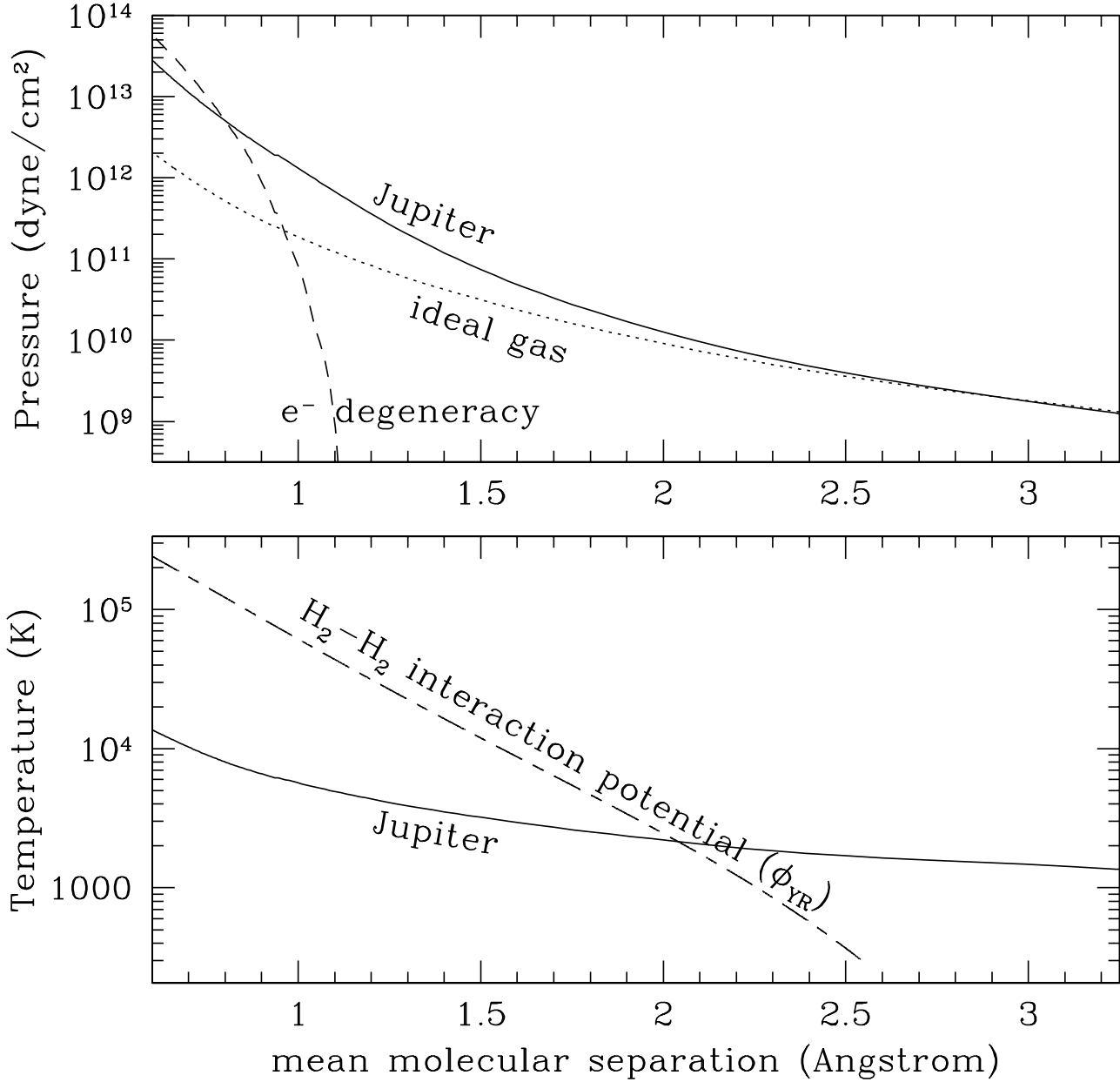


Fig. A7. The effect of $\text{H}_2\text{-H}_2$ interaction on gas pressure. The upper panel shows pressure as a function of mean molecular separation (in Å), with lower density to the right. The solid line is the actual Jupiter profile in a model from Guillot et al. (2004). The dotted line represents the ideal gas contribution (thermal pressure) { it falls short of explaining the total pressure above a pressure $p \sim 10^{10}$ dyne/cm². The dashed curve shows the contribution from electron degeneracy which only becomes important for $p \sim 10^{12}$ dyne/cm². For the in-between region, another pressure contribution has to kick in. The lower plot examines what this extra contribution is. Here, gas temperature inside Jupiter is plotted as a function of the mean separation (solid curve), while the dashed curve depicts the inter-particle potential in unit of Kelvin (the ϕ_{YR} potential from Ross et al. 1983). Molecular interaction is repulsive for a separation below 3 Å and the interaction energy becomes comparable to the thermal energy at a separation 2 Å. This contributes to the gas pressure. As density rises, the increasingly repulsive interaction dominates the gas pressure and causes the pressure to rise with density more steeply than that of an ideal gas.

while below this layer, the turbulent viscosity is significantly reduced and τ decreases sharply inward as

$$\tau \propto z^{-1}; \quad (A 3)$$

when $s = 2$ and

$$\tau \propto z^{-2} = z^{-3}; \quad (A 4)$$

when $s = 1$. These approximate scalings are shown in Fig. A8 for Jupiter models B & D. They compare well with numerical results.

b. tidal overlap in a constant density sphere

In a constant density sphere, $m = 2$ inertial modes are expressed in the following form (Paper I)

$$\delta \rho = \frac{\Omega^2}{1P} = AR^2 \frac{\Omega^2}{1P} P_{\ell}^2(x_1) P_{\ell}^2(x_2); \quad (B 1)$$

where $A \ll 1$ stands for the dimensionless amplitude of $\delta \rho$, and R is the radius of Jupiter. This density perturbation is related to the equilibrium tide value $\delta \rho_{\text{equi}}$ as

$$\frac{\delta \rho}{\delta \rho_{\text{equi}}} = \frac{2}{3} \frac{\Omega^2}{\Omega_{\text{Io}}^2} \frac{M_J}{M_{\text{Io}}} A (1 - \ell^2) g_1(x_1) g_2(x_2); \quad (B 2)$$

where Ω_{Io} 's orbital frequency $\Omega_{\text{Io}} = (GM_J/a^3)^{1/2}$, M_J and M_{Io} are the masses of Jupiter and Io, and the dimensionless frequency $\ell = \Omega/\Omega_{\text{Io}} = 0.766$. The function $g_i(x_i) = P_{\ell}^m(x_i) = (1 - x_i^2)^{\ell/2}$ (introduced in Paper I).

Pressure in a constant density ($\rho = \rho_0 = \text{const}$), self-gravitating sphere is given by $p = p_0 [1 - (r/R)^2]$ where $p_0 = 2/3 GR^2/\rho_0 = 3/8 GM^2/R^4$ with M being the total mass. Since $[1 - (r/R)^2] = (x_1^2 - x_2^2)/(x_1^2 + x_2^2) = (1 - \ell^2)/(1 + \ell^2)$, and volume elements in Cartesian coordinates and ellipsoidal coordinates are related to each other as $dx_1 dx_2 dz = (x_1^2 - x_2^2)/(1 - \ell^2) dx_1 dx_2 dz$, we obtain the following tidal overlap,

$$\delta \rho_{\text{tide}} d^3r = \frac{9}{4} \frac{\Omega^2 R^5 M_{\text{Io}}}{1a^3} A \frac{(1 - x_1^2)(1 - x_2^2)(x_1^2 - x_2^2)}{(1 - \ell^2)(x_1^2 - x_2^2)(1 - \ell^2 + x_2^2)} P_{\ell}^2(x_1) P_{\ell}^2(x_2) dx_1 dx_2 dz; \quad (B 3)$$

The spatial integration can be symbolically performed by Mathematica (best done after conversion to spherical coordinates) and it yields $0.4(1 - \ell^2) = 0.4(1 - \ell^2) \int_0^1 \int_0^1 \int_0^1 dz$. So the overlap is

$$\delta \rho_{\text{tide}} d^3r = 0.4 \frac{9}{4} \frac{\Omega^2 R^5 M_{\text{Io}}}{1a^3} A \frac{(1 - \ell^2)}{1a^3}; \quad (B 4)$$

However, the constant density case is pathological: the value of $1a$ formally approaches infinity for incompressible fluid. Inertial modes could not cause any density fluctuation (eq. B1) and the tidal overlap is formally zero.¹⁶

If we take $p = \text{constant}$ over the entire sphere (so $1a$ is a finite constant), only two modes have non-zero overlap with the tidal potential: the equilibrium tide and the two lowest order even-parity inertial modes with $\ell = 4$. This fact has been pointed out in Papaloizou & Savonije (1997) when they considered the convective core of early-type stars.

c. tidal overlap in a single power-law model

Are inertial modes in power-law models coupled to the tidal potential?

In paper I, we show that one can obtain exact solutions for inertial modes when the density profile is a single power-law $\rho \propto [1 - (r/R)^2]^{-\ell}$. This allows us to show that inertial modes in single power-law models do not couple appreciably to the tidal potential, except for the two lowest order even-parity modes (corresponding to the $\ell = 4$ modes in the constant density case).¹⁷ Moreover, the coupling strength falls off with increasing mode order as a power-law with the index related to the polytropic index.

The angular dependence of each even-parity, $m = 2$ inertial mode can be decomposed into

$$C_{\ell}(r) = \sum_{\ell=2}^{\infty} P_{\ell}^2(x_1) P_{\ell}^2(x_2) C_{\ell}(r); \quad (C 1)$$

where

$$C_{\ell}(r) = \sum_{\ell=2}^{\infty} P_{\ell}^2(x_1) P_{\ell}^2(x_2) P_{\ell}^2(\ell) \sin \ell \theta \quad (C 2)$$

is non-zero for $\ell = 2$. $C_{\ell}(r)$ is an oscillating function of the radius r . We find numerically that $C_2(r) \propto r^2$ near the center, while near the surface $C_2(r)$ approaches a constant for $\ell > 1$, and $\rho \propto [1 - (r/R)^2]^{-1/(1+\ell)}$ for $0 < \ell < 1$. The tidal overlap integral is reduced to the following radial integral,

$$\delta \rho_{\text{tide}} \frac{\Omega^2}{1P} d^3r = \frac{32}{15} \frac{3GM_{\text{Io}}}{2a^3} \Omega^2 \int_0^R D_2(r) dr = \frac{32}{15} \frac{3GM_{\text{Io}}}{2a^3} \Omega^2 \int_0^R C_2(r) \frac{r^2}{1P} dr; \quad (C 3)$$

¹⁶ The equilibrium tide, on the other hand, has finite tidal overlap. It is equivalent to an inertial mode with $\ell = 2$ so its spatial overlap diverges near the surface as p approaches 0, counteracting the formally infinite $1a$.

¹⁷ If we adopt conventional polytropic models with $p \propto \rho^{1+1/n}$, we can obtain approximate solution for the inertial modes (Paper I). We find that they give essentially the same tidal overlap results as single power-law models of the same n .

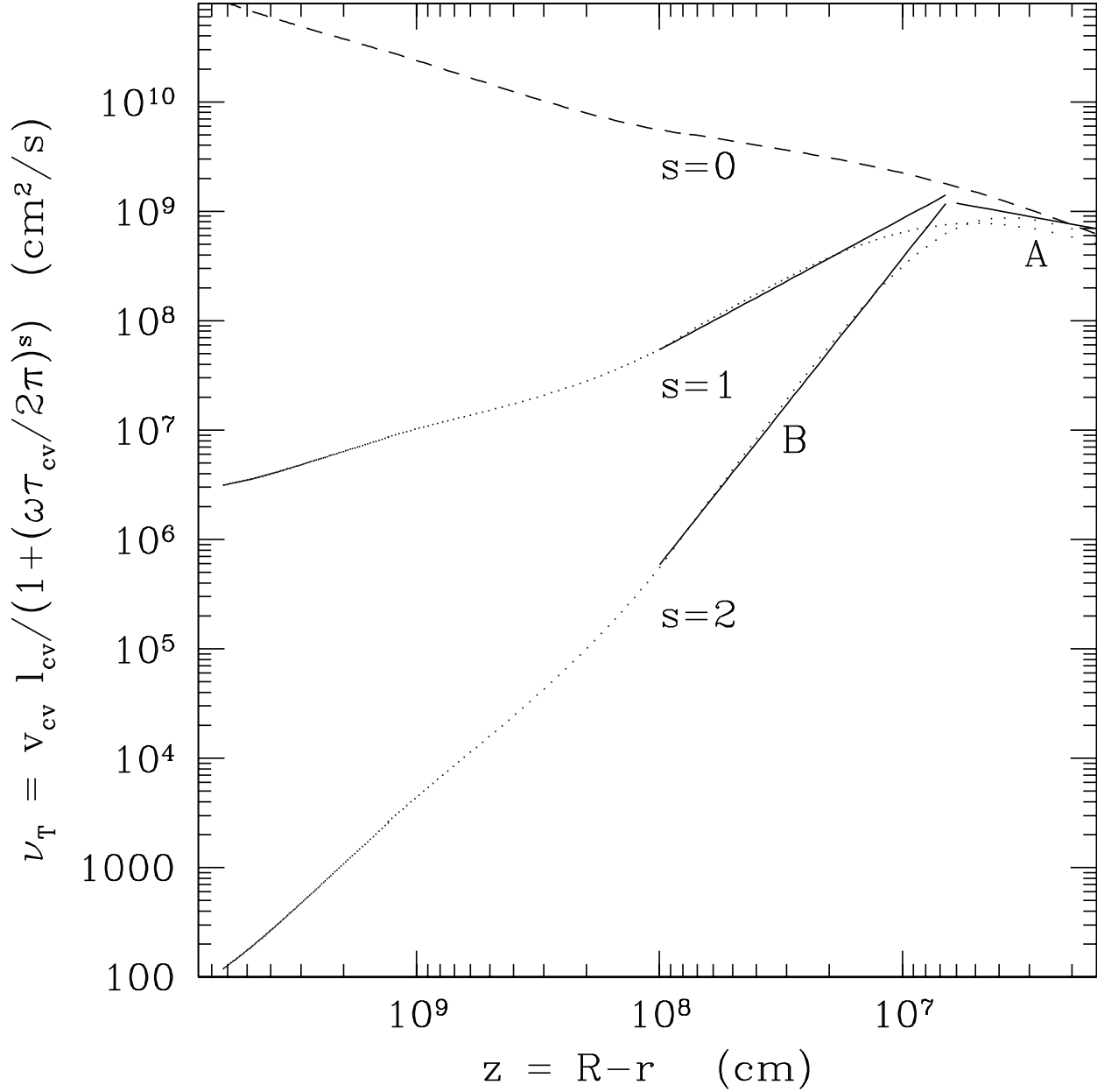


Fig. A8. The effective turbulent viscosity ν_T is plotted here as line dots against depth (z) for the Jupiter model, when various s values are adopted. The dashed curve ($s = 0$) is the un-reduced turbulent viscosity (corresponding to $s = 0$). The reduced viscosity (dotted curves) deviate from this curve below a depth $z_{\text{crit}} = 10^{2.8} R = 10^7$ cm at which $\beta_{\text{cv}} = 2 - 1$. Above z_{crit} , the viscosity is well described by line A: $\nu_T = 2 \cdot 10^0 (z=R)^{1-3} / z^{0.4}$ (with $\beta = 1.8$ in the model). Below this depth, reduction is important and $\nu_T = 4 (z=R)^{-1} / z^{2.8}$ for $s = 2$ (straight line B) and $\nu_T = 3 \cdot 10^0 (z=R)^{-2-3} / z^{1.2}$ for $s = 1$. Deeper down ($z > 10^8$ cm), as β value is varied from 1.8 to 1, ν_T takes on a different scaling with depth. However, this is irrelevant as turbulent dissipation from the deep interior is insignificant.

where we have introduced the integrand $D_2(r) = r^4 C_r(r)^2 = p$. It is also an oscillating function of r with an envelope that scales as r^6 near the center, and scales near the surface as $[1 - (r/R)]^{-1}$ for $\beta = 1$, and as $[1 - (r/R)]^{2-(\beta+1)}$ for $0 < \beta < 1$. So this integral diverges near the surface if $\beta < \frac{1}{2}$.

We find that the integral decreases with increasing mode order in a power-law fashion with the index depending on β . In the following, we explain the observed falloff with a simple toy-model.

We approximate $D_2(r)$ as a product of a rapidly oscillating function and a slowly varying envelope. A rather accurate form turns out to be

$$D_2(r)dr = \cos(n\theta) f(\theta) d\theta; \quad (C4)$$

where the new variable $\theta = \cos^{-1} r/R$, n is an integer and is the number of radial nodes in $D_2(r)$. We find $n = n_1 + n_2$ for the inertial modes. The smooth function $f(\theta)$ has a leading term of $(\theta^2)^6$ near the center ($\theta = 2$) and a leading term of $(\theta^2)^{-1}$ near the surface ($\theta = 0$).¹⁸ For the moment we assume 2 is an integer, and that terms of order 2 and higher also exist near the surface.

Integrating-by-part yields

$$\begin{aligned} \int_0^R D_2(r) dr &= \int_0^2 \cos(n\theta) f(\theta) d\theta \\ &= \frac{\sin(n\theta) f(\theta)}{n} \Big|_0^2 - \frac{\cos(n\theta) f'(\theta)}{n^2} \Big|_0^2 + \frac{\sin(n\theta) f''(\theta)}{n^3} \Big|_0^2 - \frac{\cos(n\theta) f'''(\theta)}{n^4} \Big|_0^2 + O\left(\frac{1}{n^5}\right); \end{aligned} \quad (C5)$$

So the value of this integral depends only on behavior of the function $f(\theta)$ at the two boundaries. When n is an even integer, only odd-order derivatives enter the above expression and we obtain the following results for the tidal integral,

$$\begin{aligned} \int_0^R D_2(r) dr &= \frac{f^{(2-1+M \bmod 2)}(0)}{n^{2+M \bmod 2}}; & \text{if } 2 \leq n < 7 \\ &= \frac{f^{(7)}(0)}{n^8}; & \text{if } 2 \leq n < 7 \end{aligned} \quad (C6)$$

where $f^{(2-1)}(0) = d^{2-1}f/d\theta^{2-1}|_{\theta=0}$ and so on. When 2 is odd, the above scaling depends on the fact that near the surface, terms scaled as $(\theta^2)^{-1}$ and higher also exist. If they do not (as in the left panel of Fig. C9), $1/n^8$ scaling prevails.

When n is an odd integer, slightly different scalings apply:

$$\begin{aligned} \int_0^R D_2(r) dr &= \frac{f^{(2-1+M \bmod 2-1)}(0)}{n^{2+M \bmod 2-1}}; & \text{if } 2 \leq n < 7 \\ &= \frac{f^{(6)}(0)}{n^7}; & \text{if } 2 \leq n < 7 \end{aligned} \quad (C7)$$

We have confirmed these scalings numerically with a range of expressions for $f(\theta)$. The result only depend on the boundary behavior of $f(\theta)$ as long as it is sufficiently smooth.¹⁹ This explains why models with different polytrope representations ($p/[1 - (r/R)]$ or $p/[1 + r^2]$) give rise to essentially the same overlap integrals. Moreover, when β is a fractional number (other than an integer or a half-integer), we find numerically that the above expression still applies.

Recall that the angular integration to yield $C_2(r)$ already involves a cancellation of order $1/n$.²⁰ Moreover, even-parity modes implies $n = n_1 + n_2$ to be an even number. So for the following three power-law models, $\beta = 1.0$, $\beta = 1.5$ and $\beta = 1.8$, we expect that the overall tidal overlap falls off with n as n^{-3} , n^{-5} and $n^{-4.6}$, respectively. These analytical expectations are plotted in Fig. C9 along with numerical results. The agreement is reasonable, both when integrating using the toy model ($f(\theta) \cos(n\theta)$) and when integrating using realistic inertial mode eigenfunctions.

In obtaining results like those presented in Fig. C9, one needs to be extremely careful with numerical precision. Round-off errors in the numerically produced power-law models as well as in the inertial mode eigenfunctions may occult the cancellation and lead to artificially large coupling.

d. tidal overlap in other models

The derivation leading to equation (C5) assumes that the integrand $f(\theta)$ is sufficiently smooth. What is ‘sufficiently smooth’ and in what situation does this assumption break down? It turns out that the break-down occurs for realistic planet models and that the tidal overlap is much larger than what one obtains for single power-law models.

The smoothness assumption is violated if $f(\theta)$ has a discreet jump inside the planet. Such a discontinuity is caused by the density discontinuity associated with a first-order phase transition region (e.g., gas-to-metallic hydrogen phase transition region at $r/R \approx 0.80$). Let the jump be Δf at $\theta = \theta_0$. It contributes a term, $\Delta f \sin(n\theta_0)/n = \Delta f/n$, to the tidal overlap. Even if Δf is small, this term may dominate for high order modes. Similar reasoning applies if $f(\theta)$ exhibits a discontinuity at a higher order derivative, for instance, if the above mentioned phase transition is of second

¹⁸ Here, we focus only on models with $\beta > 1$

¹⁹ In Appendix D, we discuss what the meaning of ‘sufficiently smooth’ is.

²⁰ This is so because the functional value at one of the two boundaries (the equator) is not zero (see Eq. (C5)).

order in nature so that a discontinuity in the gradient of density exists. In this case, the contribution to the overlap integral is of order $f_0 = n^2$.

The smoothness assumption can also be violated if $f(r)$ is infinitely continuous yet it (or one of its derivatives) has a sharp transition over a small region, namely, if this transition occurs over a width of Δr which encompasses only one node or less ($n \Delta r = 2\pi$). This can be caused by, e.g., a relatively sharp power-law index change inside the planet. As is discussed in xA, gas pressure inside Jupiter changes its nature from that of an ideal gas to that of strongly interacting molecules around $r = R = 0.98$. Here we observe a variation in the polytropic index over one pressure scale height, or over a thickness of $\Delta r = R = 0.002$. Within this narrow region, $f_0(r)$ varies rapidly for an amount f_0 , and $f^{(2)}(r)$ has a peak value of f_0 . The overlap integral

$$\int_0^Z \cos(nr) f(r) dr = \frac{\sin(nr) f(r)}{n} \Big|_0^Z + \frac{\cos(nr) f_0(r)}{n^2} \Big|_0^Z - \frac{1}{n^2} \int_0^Z \cos(nr) f''(r) dr; \quad (D1)$$

can be dominated by the last term and yields $f_0 = n^2$ if $n \Delta r = 2\pi$, or $n = 1/0.002 = 500$. For $n = 500$, $f(r)$ can be considered as sufficiently smooth and the analysis in Appendix C applies.

We numerically confirm these conclusions by integrating $f(r) \cos(nr)$ using a range of density profiles. Here, we take $f(r) = r^{6p_{\text{surf}}/2} = p dr/d$, where p_{surf} is $[1 - (r/R)^2]$ with the value taken at the surface. This $f(r)$ has the same asymptotic behavior as $D_2(r)$ near both boundaries.

We show that when a density discontinuity is superimposed to a single power-law model (dotted curves in Fig. D10), the overlap integral indeed scales as $1/n$. Also, if the model has a sharp (but continuous) transition in the value of p over a radius of Δr (dashed and solid curves in Fig. D10), the integral scales as $1/n^2$ for $n \Delta r = 2\pi$, while for higher n values, it behaves as is predicted by equation (C7). We have also studied integration results for two realistic Jupiter models taken from Guillot et al. (2004) (models B & D). Model D has a first-order phase transition (dotted curve in Fig. D11) and so its overlap integral scales as $1/n$; while the same phase transition is considered to be second-order in model B, and the resulting discontinuity in density gradient (as well as the equation of state transition at $r = R = 0.98$, see Appendix A.1) causes the integral to scale as $1/n^2$.

When the density profile is not a single power-law (as is the case in this section), we could not solve for inertial mode eigenfunctions exactly. We could only obtain an approximate solution that is good to the second order in wavenumber ($O(n^{-2})$, see Paper I). It is reasonable to suspect that the overlap results obtained by integrating such an approximate solution deviate from the true one. A definite answer to this suspicion will likely be provided by full numerical solution. However, we argue below that the deviation should be unimportant.

The result of integrating a fast oscillation function, as is shown in this section and Appendix C, depends only on the boundary behavior and interior discontinuities in the envelope of such a function. It does not depend on the exact shape of the function in the interior. Our approximate solution to the inertial modes is exact near the surface, and is sufficiently accurate near the center (where the WKB approximation works well). Moreover, when a density discontinuity (or discontinuity in density derivatives) is present inside the WKB region, as inertial modes are insensitive to density structure, the solution is not expected to deviate qualitatively from the approximate solution that included

In confirming the scalings derived in this section, we have only integrated the toy-model ($f(r) \cos(nr)$), instead of integrating inertial mode eigenfunctions (in Fig. C9 we integrate both). One can similarly argue that integrating an appropriately chosen $f(r)$ is equivalent of integrating the real function. In fact, our toy model should produce results both qualitatively and quantitatively similar to that obtained using the actual eigenfunctions, one can almost make do without detailed knowledge of the latter, e.g. such a density discontinuity.

Lastly, independent of the radial profile, integration in the angular direction always introduces a factor of $1/n$ cancellation.

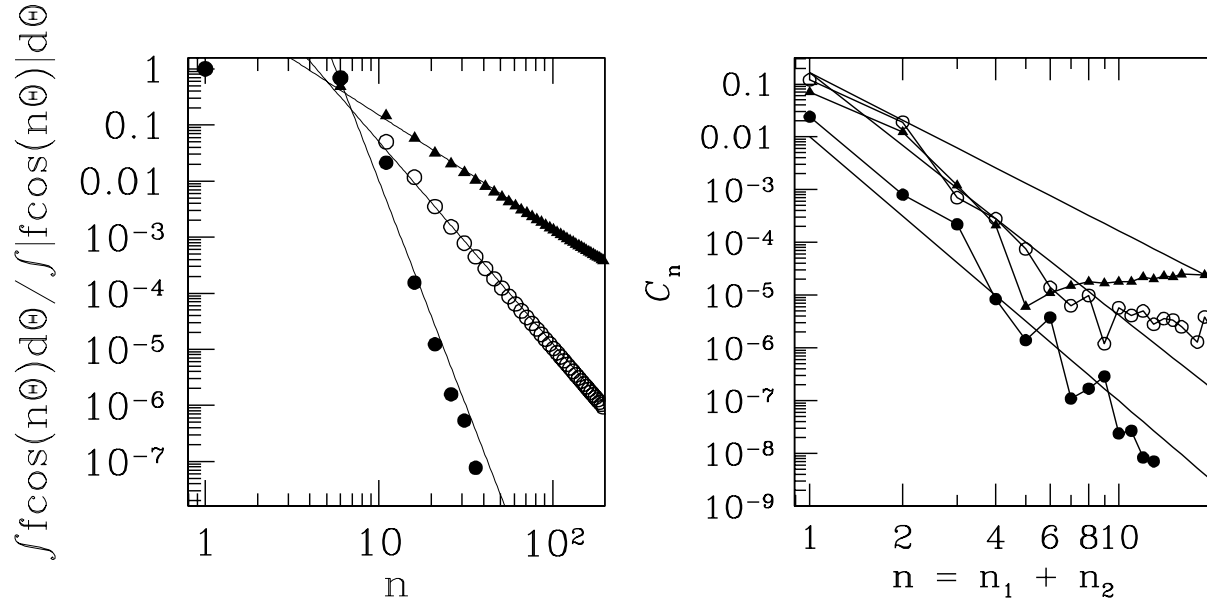


Fig. C9. Severity of cancellation in the overlap integrals as a function of mode nodal number (n where n is even) in three single power-law models (solid triangles for $\nu = 1:0$; solid circles for $1:5$ and open circles for $1:8$). The left-hand panel is the toy model result where we have taken the envelope of the cosine function (eq. C4) to be $f(\Theta) = f_0 r^6 \sin^2 \Theta$ where $\Theta = \cos^{-1} r/R$. This allows the toy model tidal integrand to have the correct asymptotic behavior as the realistic tidal integrand both near the center and near the surface. The severity of cancellation is measured here by $|\int f \cos(n\Theta) d\Theta| / |\int f \cos(n\Theta) d\Theta|$ and it scales as (solid lines) n^{-2} , n^{-8} and $n^{-3/6}$, respectively, for the three models, consistent with results in equation C6). The right panel is the severity of cancellation C_n (eq. B1) calculated for inertial modes in the same three models. Again, the three straight lines are the analytically expected scalings, n^{-3} , n^{-5} and $n^{-4/6}$, respectively, for the three models. The extra power of n compared to those for the toy model arises from cancellation in the angular direction, except for the $\nu = 1:5$ model, which does not fall off as n^{-9} due to the presence of $\sin^3 \Theta$ term near the surface. Results in the $\nu = 1:0$ model first deviates from the scaling but returns to it at large n and the $\nu = 1:5$ model falls off more steeply than the $\nu = 1:8$ model, as is expected.

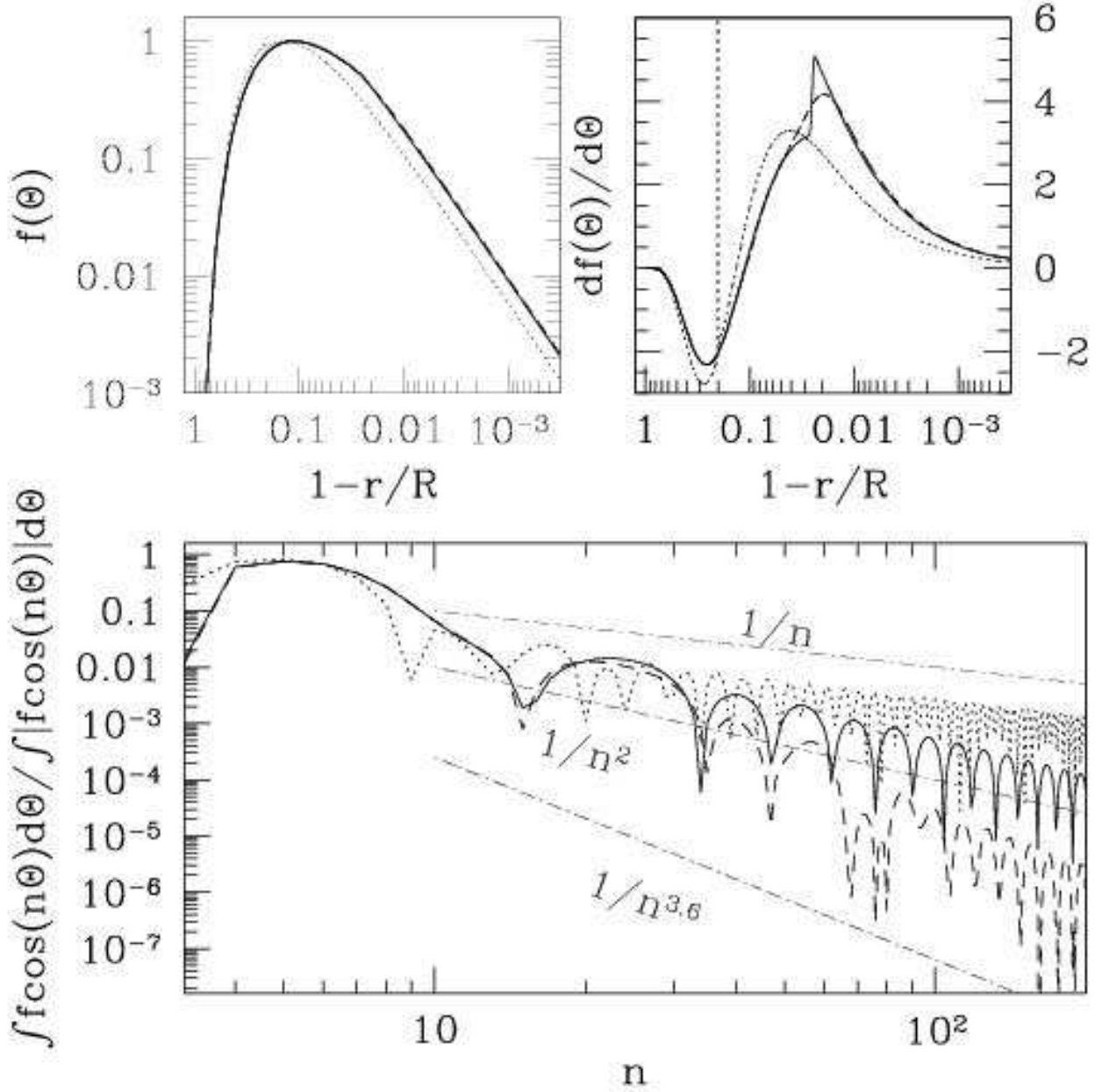


Fig. D10. The severity of cancellation in the overlap integral calculated using the toy model for three different density profiles are shown in the lower panel as a function of n (n even), while the top two panels show the corresponding $f(\theta)$ (left) and $df/d\theta$ (right) as functions of $1-r/R = 1 - \cos \theta$. We take $f(\theta)$, the envelope of the cosine function to be $f(\theta) = \hat{f}^2 \rho(r) = \hat{f}^2 \rho(r) r^2$ while the various density profiles are: a $\rho = 1.8$ power-law model, overlaid with a 1% density jump at $r/R = 0.8$ (dots, exhibiting a δ -function in $df/d\theta$); a mock Jupiter model where the power-law index varies from 1 in the interior to 1.8 in the envelope, with the transition occurring at $r/R = 0.98$ (solid lines, having a jump in $df/d\theta$) and spanning a range of $r/R = 0.002$ (FWHM of the spike in $d^2f/d\theta^2$); a similar model but with the transition occurring over a range of $r/R = 0.02$ (dashed curves, the one with smooth $df/d\theta$). Analytically, we expect scalings of $1/n$, $1/n^2$ switching to $1/n^{3.6}$ when $n > 500$, and $1/n^2$ switching to $1/n^{3.6}$ when $n > 50$, for the three models, respectively. These scalings are marked here as the three dot-dashed lines.

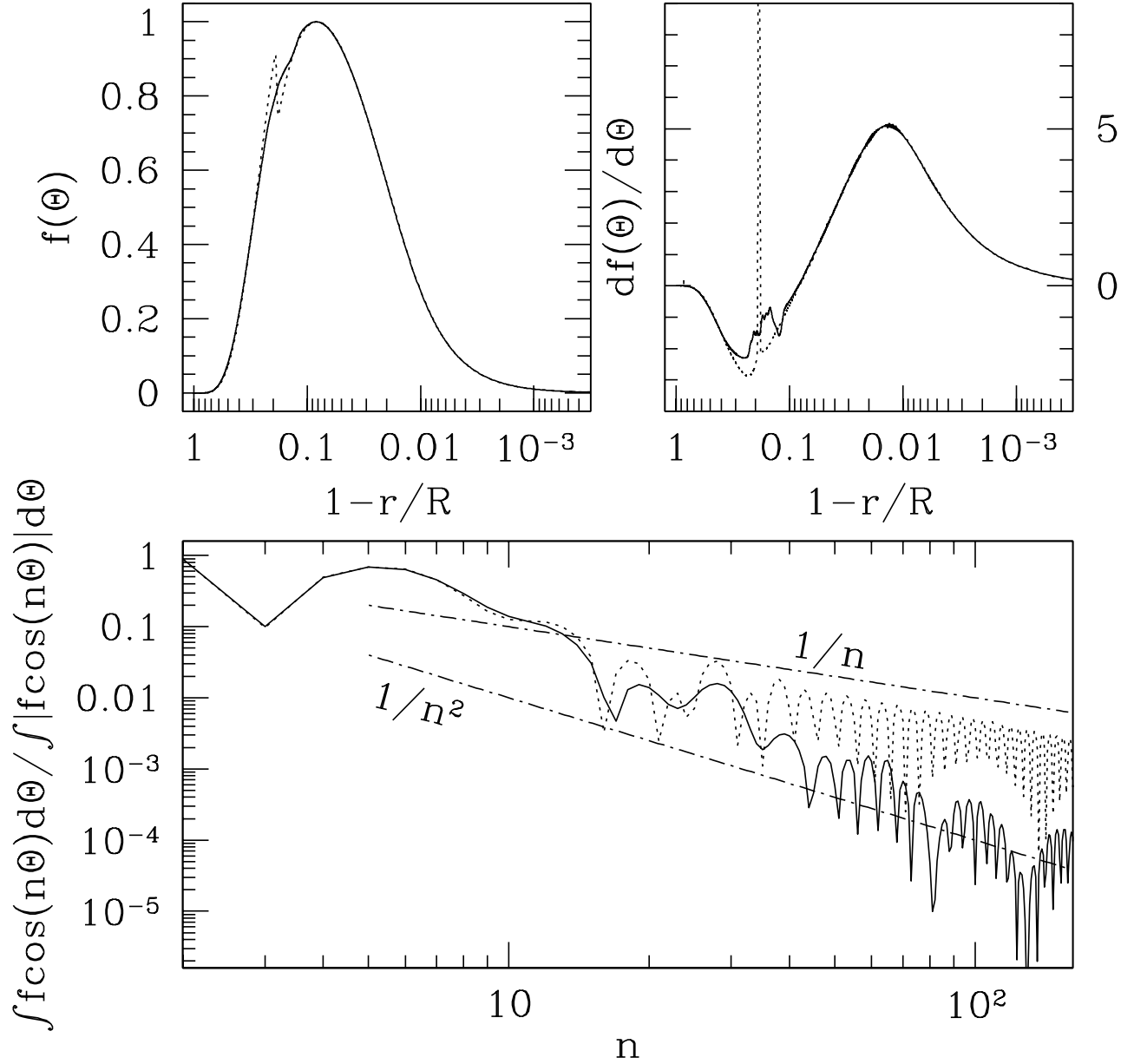


Fig. D11. Same as Fig. D10 but with the density profile taken from two realistic Jupiter models: models B & D as in Guillot et al. (2004). Model B (solid curves) is based on an interpolated equation of state with no core and no density discontinuity across the metallic hydrogen phase transition region at $r=R-0.8$ (but the first derivative of density is discontinuous there (df/dr jumps by $\sim 50\%$)). Overlap integral in model B is expected to suffer a cancellation with a $1/n^2$ scaling (lower panel). The sharp transition in the equation of state around $r=R-0.98$, with a FWHM for df/dr of $r=R-0.02$, also contributes to this scaling. But this contribution falls off sharply for $n-1=0.02-50$. Model D (dotted curves) has a $10M_{\oplus}$ solid core, and is based on PPT equation of state with the phase transition being first-order, giving rise to a fractional density jump of $\sim 20\%$. This is seen here as the jump in $f(\Theta)$ and the spike in df/dr . Overlap integral in model D is dominated by the density jump and it scales roughly as $1/n$, as expected. These results are insensitive to core sizes, since the r^6 scaling in $f(\Theta)$ near the center suppresses any influence from the inner boundary condition. Moreover, severity of cancellation calculated for actual inertial-mode eigenfunctions is expected to be one power of n steeper than those presented here, due to cancellation in the angular direction.